Petrogenesis of Volcanic Rocks from Saipan and Rota, Mariana Islands, and Implications for the Evolution of Nascent Island Arcs

MARK K. REAGAN[1]*, BARRY B. HANAN[2], MATTHEW T. HEIZLER[3], BRIAN S. HARTMAN[1] AND ROSEMARY HICKEY-VARGAS[4]

[1]DEPARTMENT OF GEOSCIENCE, UNIVERSITY OF IOWA, IOWA CITY, IA 52242, USA

[2]DEPARTMENT OF GEOLOGICAL SCIENCES, SAN DIEGO STATE UNIVERSITY, SAN DIEGO, CA 92182, USA

[3]NEW MEXICO BUREAU OF MINES AND MINERAL RESOURCES, NEW MEXICO INSTITUTE OF TECHNOLOGY, 801 LEROY PLACE, SOCORRO, NM 87801, USA

[4]DEPARTMENT OF EARTH SCIENCES, FLORIDA INTERNATIONAL UNIVERSITY, MIAMI, FL 33199, USA

RECEIVED OCTOBER 1, 2006; ACCEPTED DECEMBER 19, 2007
ADVANCE ACCESS PUBLICATION JANUARY 30, 2008

An $^{40}Ar/^{39}Ar$ age of 45·1 Ma determined for lavas from northern Saipan confirms that these high-silica rhyolites erupted during the 'proto-arc' stage of volcanism in the Izu–Bonin–Mariana system, which is characterized elsewhere by eruption of boninitic lavas. Incompatible trace element concentrations and Sr, Hf, Nd, and Pb isotope ratios for these rhyolites are transitional between those of c. *48 Ma boninitic lavas and post-38 Ma 'first-arc' andesites and dacites from Saipan and Rota that have typical subduction-related compositions. These transitional compositions are modeled by crystal fractionation of parental tholeiitic basalt combined with assimilation of young boninitic crust. A second stage of Rayleigh fractionation in the upper crust is required by SiO_2 concentrations that exceed 77 wt % and near-zero compatible element concentrations. First-arc magma compositions are consistent with fractionation of basalt and assimilation of crust similar in composition to the first-arc magmas themselves. The mantle sources of the proto-arc and first-arc lavas from Saipan and Rota are similar to those of Philippine back-arc basin basalts based on Nd and Hf isotopic compositions. The Pb isotope compositions of these lavas are between those of Pacific sea-floor basalts and Jurassic and younger cherty and clay-rich sediments. This contrasts with the boninitic proto-arc volcanic rocks from Guam and Deep Sea Drilling Project Sites 458 and 459 that have Pb isotope compositions similar to Pacific basin basalts and volcaniclastic sediments. The preferred explanation for the difference in the nature of proto-arc volcanism between Saipan and other fore-arc locations is that the crust ceased extending 3–4 Myr earlier beneath Saipan. This was caused by a change from mantle upwelling, fore-arc extension, and shallow melting to an environment dominated by more normal mantle wedge convection, stable crust, and deeper melting.*

KEY WORDS: *rhyolite; andesite; Mariana arc; isotope ratios; trace elements*

INTRODUCTION

The majority of Quaternary oceanic island arc volcanoes, including those in the modern Mariana arc, rarely erupt rhyolites. This is commonly presumed to result from the inability of parental mafic magmas to differentiate to silicic residua in the relatively thin, mafic, and dense crust of oceanic island arcs. Nevertheless, large-scale rhyolitic volcanism is a characteristic of the modern Izu arc (e.g. Tamura & Tatsumi, 2002) and analyses of volcaniclastic sediments drilled by the Deep Sea Drilling Project (DSDP) and Ocean Drilling Program (ODP) show that rhyolitic volcanism has occurred throughout the history of the Izu–Bonin–Mariana (IBM) system of arcs (Bryant *et al.*, 1999; Tamura & Tatsumi, 2002; Straub, 2003; Shukuno *et al.*, 2006). Furthermore, the IBM system has been shown to have a mid-crustal layer of variable

*Corresponding author. Telephone: 1-319-335-1802. Fax: 1-319-335-1821. E-mail: mark-reagan@uiowa.edu

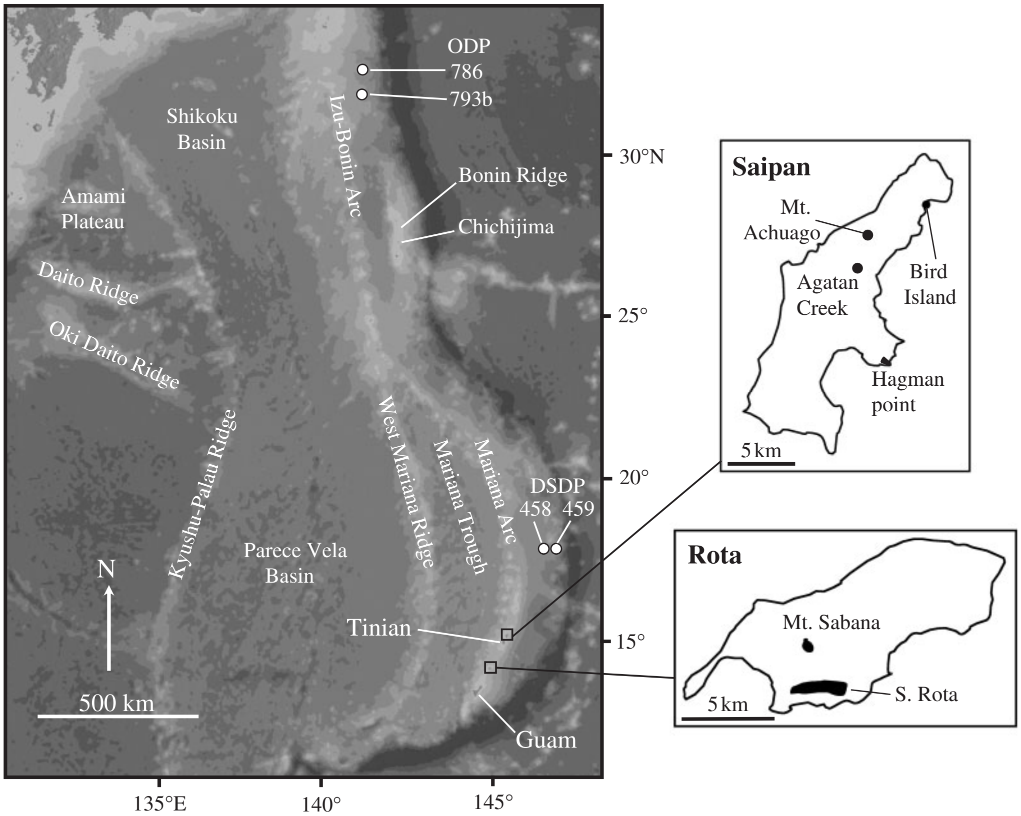

Fig. 1. Location map for the Izu–Bonin–Mariana arc system. Base map was constructed using GeoMapApp.

thickness with seismic velocities consistent with the presence of tonalite and associated plutonic materials (Suyehiro *et al.*, 1996; Takahashi *et al.*, 1998, 2007).

The oldest recognized rhyolitic lava and tephra sequences in the IBM system are middle Eocene in age and make up the core of the island of Saipan (Cloud *et al.*, 1956). These volcanic rocks are enigmatic in that they are high-Si rhyolites with 'mature' arc major element, trace element and Sr–Nd–Pb isotopic compositions, despite having erupted during the 'proto-arc' (Pearce *et al.*, 1999) phase of volcanism in the IBM system, which is dominated elsewhere by boninite series lavas and bronzite andesites (Tracey *et al.*, 1964; Meijer *et al.*, 1983; Reagan & Meijer, 1984; Umino, 1985; Dobson, 1986; Taylor *et al.*, 1994; Ishizuka *et al.*, 2006).

To better understand the petrogenesis of the rhyolites from Saipan, selected samples were analyzed for their major and trace element and Sr, Hf, Nd, and Pb isotope composition. These data are compared with similar data for younger andesites and dacites collected from Saipan and Rota, as well as literature data for proto-arc volcanic rocks from throughout the IBM system, to understand the origin of rhyolitic magmatism on Saipan in the context of the overall evolution of the IBM system.

REGIONAL GEOLOGY

The southern IBM system includes, from east to west, the Mariana Trench, the Mariana fore-arc (including the islands of Saipan, Rota, and Guam), the active Mariana arc, the Mariana Trough, the West Mariana Ridge, the Parece Vela Basin, and the Kyushu–Palau Ridge (Fig. 1). Proto-arc sequences range in age from *c.* 48 to 44 Ma and are exposed along the Kyushu–Palau Ridge and in the IBM fore-arc (e.g. Meijer *et al.*, 1983; Cosca *et al.*, 1998; Pearce *et al.*, 1992, 1999; Ishizuka *et al.*, 2006). The oldest arc rocks in the IBM system are predominantly boninitic (Reagan & Meijer, 1984; Cosca *et al.*, 1998; Mohler, 2003; Reagan *et al.*, 2003; Taylor *et al.*, 1994). The combination of high SiO_2 and MgO contents together with low concentrations of rare earth elements (REE) in the boninites are commonly inferred to have resulted from hydrous melting of mantle at unusually low pressures and to unusually high extents (Green, 1973; Falloon & Danyushevsky, 2000; Parman & Grove, 2004). Catastrophic failure of the Pacific plate and subduction initiation probably caused these unusual conditions of melting (Stern & Bloomer, 1992; Hall *et al.*, 2003; Stern, 2004).

Some silicic volcanic rocks, including rhyolites, are interbedded with boninites at ODP Site 786, and rhyolite dikes cut through the entire sequence of boninitic volcanic rocks on Chichijima. These rhyolites have variable SiO_2 concentrations and appear to be geochemically related to the boninites (Pearce *et al.*, 1992; Taylor *et al.*, 1994). We demonstrate here that the high-Si rhyolites on Saipan are distinct in composition and must have a distinct petrogenesis from other lavas of similar age elsewhere in the IBM system.

Late Eocene to Oligocene volcanism in the IBM system is marked by eruption of tholeiitic and calc-alkaline basalts, andesites, dacites and rhyolites with trace element characteristics that are typical for subduction-related lavas; that is, they are enriched in large ion lithophile elements and U over Th and the REE, and depleted in Nb and Ta with respect to La. These sequences have been called the 'first-arc' by Gill *et al.* (1994). First-arc rocks make up the Alutom Formation on Guam and the Hagman Formation on Saipan. As discussed below, there are also significant exposures of first-arc rocks on Rota. All of these units yield late Eocene to early Oligocene K–Ar and ^{40}Ar–^{39}Ar ages (Cosca *et al.*, 1998; this study).

GEOLOGY OF SAIPAN AND ROTA

The islands of Guam, Rota, and Saipan cap the fore-arc ridge trenchward of the active Mariana arc (Fig. 1). The geology of Saipan consists of Eocene to Miocene arc volcanic rocks overlain by, and interbedded with, limestones ranging in age from Eocene to Recent. The oldest rocks on Saipan are the rhyolite lava flows and associated volcaniclastic sequences of the middle Eocene Sankakuyama Formation (Cloud *et al.*, 1956; Meijer *et al.*, 1983; Cosca *et al.*, 1998). The type section of the Sankakuyama Formation is located on Mount Achuago in the north–central part of the island (Tayama, 1938). Southward of Mount Achuago's summit are tabular, south-dipping rhyolite flows that are interlayered with flow breccias. Flow foliations in these rhyolite sequences, along with the lack of any pillow structures or hyaloclastites, indicate that they were most probably erupted subaerially. The groundmass of the rhyolites from Mount Achuago is finely crystalline, and has dispersed millimeter-scale spherulites and irregular patches composed of microcrystalline quartz. Outcrops along the NE coast of Saipan near Bird Island are poorly sorted pyroclastic deposits with angular clasts and variable proportions of ash. The ash-poor layers often contain clasts with perlitic groundmasses, which may represent autobreccias associated with the rhyolite lavas, whereas the ash-rich layers appear to be ash-flow tuffs and related rocks. All Sankakuyama rhyolites contain 3–8% crystals of euhedral to embayed quartz and 1–3% euhedral to subhedral plagioclase up to about 1 mm in length. The only ferromagnesian minerals present are rare Fe–Ti oxides. The first-arc Hagman Formation on Saipan includes andesitic volcaniclastic rocks and lava flows (Cloud *et al.*, 1956). The samples on which this study is based were collected from coarse matrix-supported volcanic conglomerates and breccias near Hagman Point and near Agatan Creek on the slopes of Mount Talafofo. The locations for these samples and others used in this study are listed in Electronic Appendix 1, which is available for downloading at http://www.petrology.oxfordjournals.org.

The volcanic sections on Rota consist of monolithologic to polymictic breccias and conglomerates with andesite and dacite clasts. These pyroclastic units crop out in two main locations on the island. Those exposed along the southern slope of Rota, which we tentatively name here the Ogo volcanics, dip southeastward (strikes and dips of 072–081°/20–40°S) and are clast-supported to matrix-supported volcanic conglomerates with subangular to rounded cobbles and boulders (up to ~40 cm) of two-pyroxene andesite. Most clasts from the Ogo volcanics and the Hagman Formation on Saipan are dark gray to olive gray andesites with 70–90% groundmass and phenocrysts of plagioclase, clinopyroxene, orthopyroxene, and magnetite in decreasing order of abundance. Basaltic andesite breccias exposed on Mount Sabana, which we tentatively name here the 'Sabana andesite', appear to be the remnants of an eroded subaerial cinder cone. These breccias are clast-supported, poorly sorted and consist of angular to sub-angular clasts up to ~0·5 m in length. These andesites have fine-grained groundmasses that make up 50–60% of the rock. Crystalline phases are dominated by complexly zoned plagioclase with subordinate amounts of clinopyroxene, orthopyroxene, magnetite, and rare olivine crystals. Rounded websterite xenoliths up to several millimeters in diameter make up 5–10% of the samples of the Sabana andesite. These xenoliths are variably disaggregated and appear to be the source of most of the large pyroxene crystals in these lavas based on the similarities in colors, textures, and abundances of magnetite inclusions in the individual and xenolith pyroxenes. Some of the clinopyroxene crystals in these xenoliths have thin orthopyroxene exsolution lamellae, indicating that at least some of the xenoliths were once at sub-solidus temperatures. Clay and other secondary minerals replace groundmass glasses and olivine in all first-arc samples and zeolites fill vesicles in some samples from both locations.

The volcanic rocks collected from the Hagman Fm. and Ogo volcanics have compositions that are similar to those in the Alutom Fm. on Guam (see Hickey-Vargas & Reagan, 1987). In addition, the paleontologic and radiometric ages of the volcanic sequences on Rota, as well as the Hagman and Alutom formations on Saipan and Guam, appear to be identical (Meijer *et al.*, 1983; this work).

ANALYTICAL TECHNIQUES

Samples were broken into 2–5 cm fragments, hand-picked for freshness, then washed in purified water, dried,

Table 1: Summary of $^{40}Ar/^{39}Ar$ age information

Sample	Island	Unit	Material	Rock type	Wt (mg)	Plateau						Isochron							Total gas	
						Age	±1σ	MSWD	Steps	*n*	$\%^{39}Ar$	Age	±1σ	MSWD	$^{40}Ar/^{36}Ar_i$	±1σ	Steps	*n*	Age	±1σ
GUM 80-1b	Guam	Alutom	H	andesite	30·41	38·26	0·56	0·9	D–H	5	92·5	38·6	0·8	1·0	294·0	3·0	D–H	5	38·39	0·71
ROT-02-3	Rota	Ogo	GM	andesite	50·21	34·84	0·43	11·7	C–I	7	66·7	34·9	0·2	13·0	295·0	2·0	C–I	7	33·43	0·30
ROT-02-3	Rota	Ogo	P	andesite	52·35	32·43	0·86	2·6	B–H	7	72·5	33·2	0·8	3·2	291·0	4·0	B–K	10	30·66	0·93
ROT-02-8	Rota	Sabana	GM	andesite	52·32	36·00	0·36	20·4	C–I	7	68·4	36·2	0·2	22·0	290·0	4·0	C–I	7	34·74	0·19
ROT-02-8	Rota	Sabana	P	andesite	29·97	33·68	0·84	1·1	C–K	9	67·7	32·8	0·9	1·3	297·0	4·0	A–K	11	33·2	1·1
SPN02-2	Saipan	Sankakuyama	GM	rhyolite	19·99	40·68	0·60	1·1	C–H	6	48·8	36·0	2·0	3·8	302·0	2·0	C–I	7	44·7	1·5
SPN02-13	Saipan	Sankakuyama	GM	rhyolite	53·42	45·12	0·26	2·0	A–H	8	97·6	45·4	0·3	1·9	293·3	1·6	A–H	8	45·84	0·80

H, hornblende; GM, groundmass concentrate; P, plagioclase. Isochron age determined by York (1969) regression of isotope correlation data. All ages reported relative to FC-2 sanidine at 27·84 Ma. The term plateau is used to represent an age calculated by inverse variance weighting of multiple heating steps. The $^{40}Ar/^{39}Ar$ methods are described in Electronic Appendix 2.

and crushed in a Bico chipmunk. Randomized portions of the crushed samples were powdered using a ceramic shatterbox. Major elements were analyzed by inductively coupled plasma emission spectrometry (ICP-ES) at Florida International University on a Jobin-Yvon JY 70 Type III ICP-AES system using the methods described by Hickey-Vargas *et al.* (1995). Trace element concentrations were analyzed by inductively coupled plasma mass spectrometry (ICP-MS) at Boston University using a VG PlasmaQuad ExCell ICP-MS system, according to the procedures outlined by Plank & Ludden (1992), Elliott *et al.* (1997), and Kelley *et al.* (2003).

The Hf for isotopic analysis was separated using the protocol of Blichert-Toft *et al.* (1997), the Pb according to Hanan & Schilling (1989), and the Nd according to Schilling *et al.* (1994), modified by using Eichrom Ln·Spec resin. The Sr was separated in a quartz glass column using cation exchange in an HCl medium. After Sr elution, Ba was removed with 2M HNO_3 prior to eluting the REE with 6M HNO_3. The Sr fraction was purified in a Teflon column using Eichrom Sr Spec resin with an HNO_3 medium. The total analytical blanks for these procedures were <90 pg Pb, <25 pg Hf, <200 pg Sr, and <50 pg Nd. Thus no blank corrections were made. Hafnium and lead isotopic compositions were measured at Ecole Normale Superieure in Lyon using a VG Plasma 54 MC-ICPMS system following the methods described by Blichert-Toft *et al.* (1997) and White *et al.* (2000). Strontium and neodymium isotopes were analyzed by thermal ionization mass spectrometry (TIMS) and multicollector (MC)-ICPMS at San Diego State University using a VG Sector 54 and a Nu Plasma HR system, respectively. The $^{176}Hf/^{177}Hf$ and $^{143}Nd/^{144}Nd$ were normalized for mass fractionation relative to $^{179}Hf/^{177}Hf = 0{\cdot}7325$ and $^{146}Nd/^{144}Nd = 0{\cdot}7219$. The JMC-475 Hf standard was run alternately with samples to monitor machine performance. All Nd and Hf duplicate analyses agree within the analytical errors defined by replicate analyses of the JMC 475 Hf and La Jolla Nd standards. The measured $^{143}Nd/^{144}Nd$ value of 0·511844 for the La Jolla standard differs from the value of 0·51186 measured by Pearce *et al.* (1999). Therefore, the $^{143}Nd/^{144}Nd$ values from this study have been proportionally adjusted for comparison on figures. The Pb isotope ratios were corrected for instrumental mass fractionation and machine bias by applying a discrimination factor determined by bracketing sample analyses with analyses of the NIST standard SRM 981, using the SRM 981 values determined by Todt *et al.* (1996). NIST SRM 997 Tl was used to monitor fractionation (White *et al.*, 2000; Albarède *et al.*, 2004). The Pb isotope ratios for duplicates agree within the ±2σ error of the NBS 981 average.

Selected samples were dated using $^{40}Ar/^{39}Ar$ methods at the New Mexico Geochronology Laboratory. These data are listed in Table 1 and illustrated in Figs 2–5. Further information about the analytical methods is given in Electronic Appendix 2. Whole-rock samples were processed and ages were determined using the procedures outlined by Heizler *et al.* (1999). Ages were obtained from groundmass concentrates and plagioclase and hornblende mineral separates.

Major element analyses of pyroxene phenocrysts and pyroxenes in websterite xenoliths in the andesites from Mount Sabana, Rota were obtained using a CAMECA SX-50 electron microprobe at Oregon State University and techniques described by Kohut *et al.* (2006).

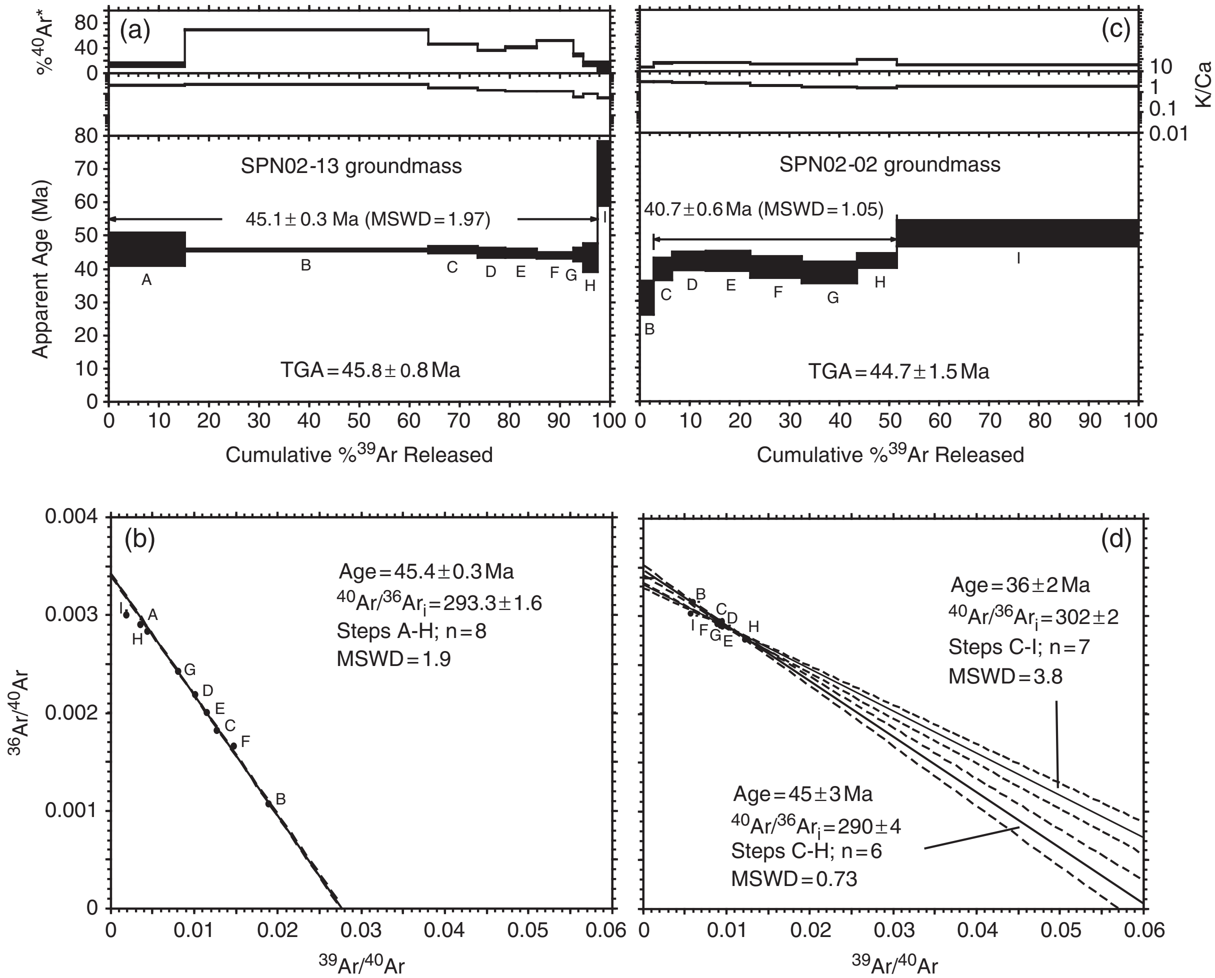

Fig. 2. $^{40}Ar/^{39}Ar$ age spectra (a, c) and isotope correlation diagrams (b, d) for groundmass from samples SPN02-13 and SPN02-02. Total gas ages (TGA) are listed in (a) and (c).

GEOCHRONOLOGY

$^{40}Ar/^{39}Ar$ incremental heating age spectrum analyses were conducted on a total of seven samples from Saipan, Rota and Guam. Complete analytical results are provided in Electronic Appendix 2 and age spectra and isotope correlation diagrams are given in Figs 2–5. These data, as well as weighted mean and isotope correlation ages, are summarized in Table 1.

Age spectra for groundmass fractions from rhyolites of the Sankakuyama Formation on Saipan are variably complex, with SPN02-13 giving a well-defined plateau age of 45·1 ±0·3 Ma and SPN02-02 yielding a somewhat disturbed spectrum (Fig. 2). The plateau age for SPN02-13 comes from the first eight heating steps, which comprise about 98% of the spectrum, with the isotope correlation diagram yielding an analytically identical age and a trapped initial $^{40}Ar/^{36}Ar$ component within error of the 295·5 atmospheric value (Fig. 2b, Table 1). SPN02-02 gives a spectrum with a flat segment (40·7 ± 0·6 Ma, MSWD = 1·05) between about 3 and 52 cumulative per cent ^{39}Ar released that is followed by a single step at about 50 Ma. The low radiogenic yield of this sample (<20%) and the data clustering on the isotope correlation diagram cause a significant dispersion of ages for different linear regressions (Fig. 2d). For instance, using the steps that define the initial flat segment (C-H) provides an apparent age of 45 ± 3 Ma and initial $^{40}Ar/^{36}Ar$ of 290 ± 4, whereas inclusion of the older step leverages the regression into the excess argon field ($^{40}Ar/^{36}Ar$ initial = 302 ± 2) and results in an apparent age of 36 ± 2 Ma (Fig. 2d; Table 1). The latter regression has an elevated MSWD of 3·8 and therefore does not define a normal distribution. Based on the quality of the two results, SPN02-13 at 45·1 ±0·3 Ma best represents the eruption age for the Sankakuyama Formation. The 45·1 Ma result is indistinguishable from a relatively imprecise 46·6 ± 1·6 Ma $^{40}Ar/^{39}Ar$ plateau age reported by Cosca *et al.* (1998) and also is consistent with the paleontological age established

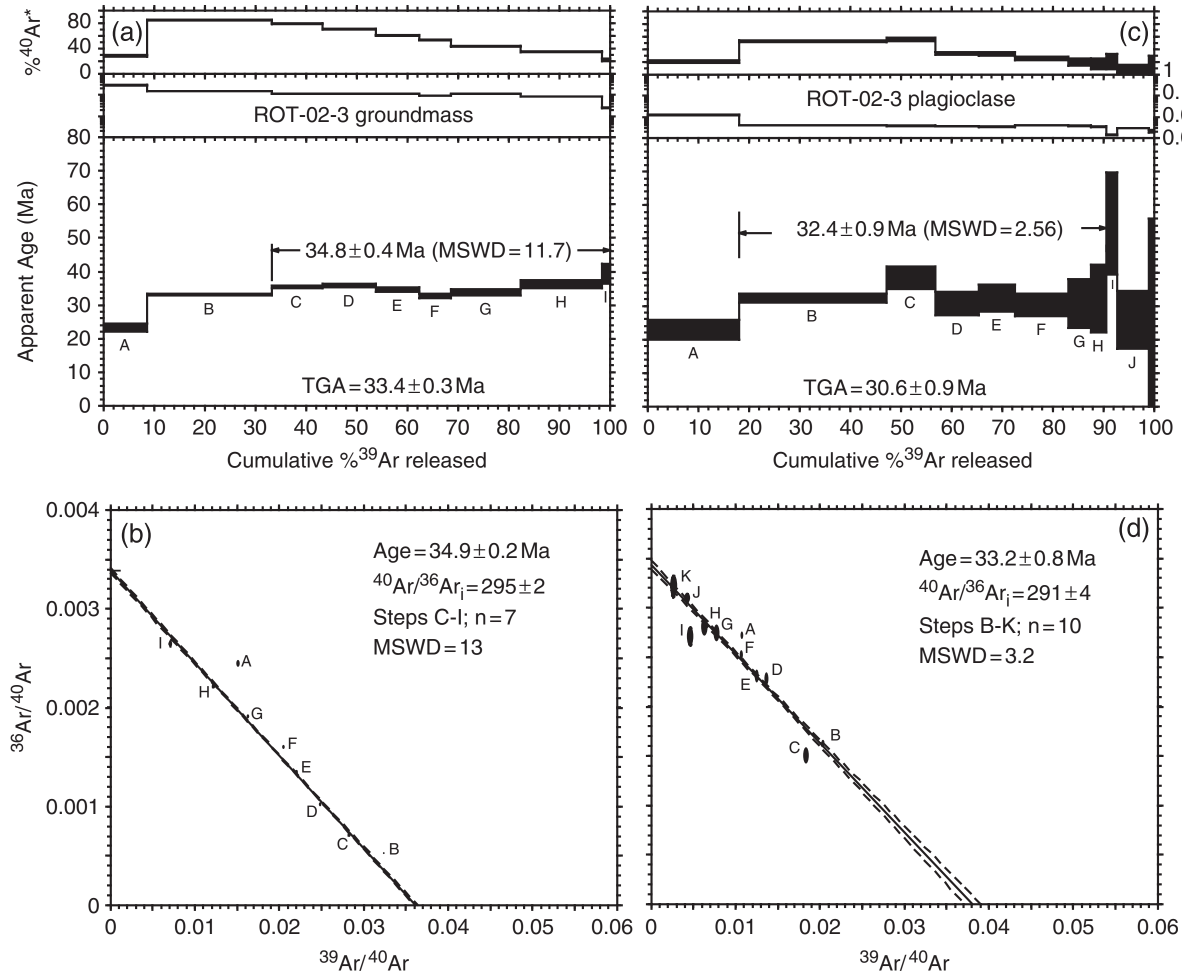

Fig. 3. $^{40}Ar/^{39}Ar$ age spectra (a, c) and isotope correlation diagrams (b, d) for groundmass and plagioclase for sample ROT02-3.

by Cloud *et al.* (1956) on the Sankakuyama Formation. This age lies between the ~48 Ma age determined for boninites from DSDP Site 458 (Cosca *et al.*, 1998) and Chichijima (Ishizuka *et al.*, 2006) and the ~44 Ma ages determined for the boninitic lavas of the Facpi formation on Guam (Meijer *et al.*, 1983; Reagan *et al.*, 2003).

Groundmass and plagioclase age spectra from andesites from Rota are significantly disturbed (Figs 3 and 4), and must be interpreted cautiously. A groundmass concentrate and a plagioclase mineral separate were analyzed from samples ROT-02-3 and ROT-02-8, which represent the Ogo volcanics and Sabana andesite, respectively. The groundmass concentrates from ROT-02-3 and ROT-02-8 have similar spectra that climb from about 25 Ma to about 35 Ma for the first *c.* 30% of ^{39}Ar released, followed by an undulatory pattern for the remaining heating steps (Figs 3a and 4a). The single steps have fairly high age precision, but the weighted mean ages calculated for the oldest part of each spectrum have high (10–20) MSWD values, indicating significant scatter. It is not possible to determine the cause of the scatter as effects related to ^{39}Ar recoil redistribution cannot be separated from possible geological issues such as argon loss or excess argon. It is possible that the oldest and youngest parts of the higher temperature steps (36 and 33 Ma) represent mixing between the eruption age and a later argon loss event caused by alteration and/or reheating (see Kuiper, 2002); however, such an interpretation would require substantiation by other means. The isotope correlation diagrams of the Rota groundmass samples display substantial scatter and do not define a simple two-component mixing between homogeneous trapped and radiogenic Ar components (Figs 3b and 4b). The plagioclase age spectra (Figs 3c and 4c) display some scatter and have low precision related to very low K contents (K_2O 0·04%). ROT-02-8 plagioclase yields a statistically robust plateau age of $33{\cdot}7 \pm 0{\cdot}8$ Ma that is indistinguishable from the more scattered weighted mean age of $32{\cdot}4 \pm 0{\cdot}9$ Ma given by the groundmass. ROT-02-3 plagioclase is slightly more disturbed compared with ROT-02-8 plagioclase but yields a weighted mean

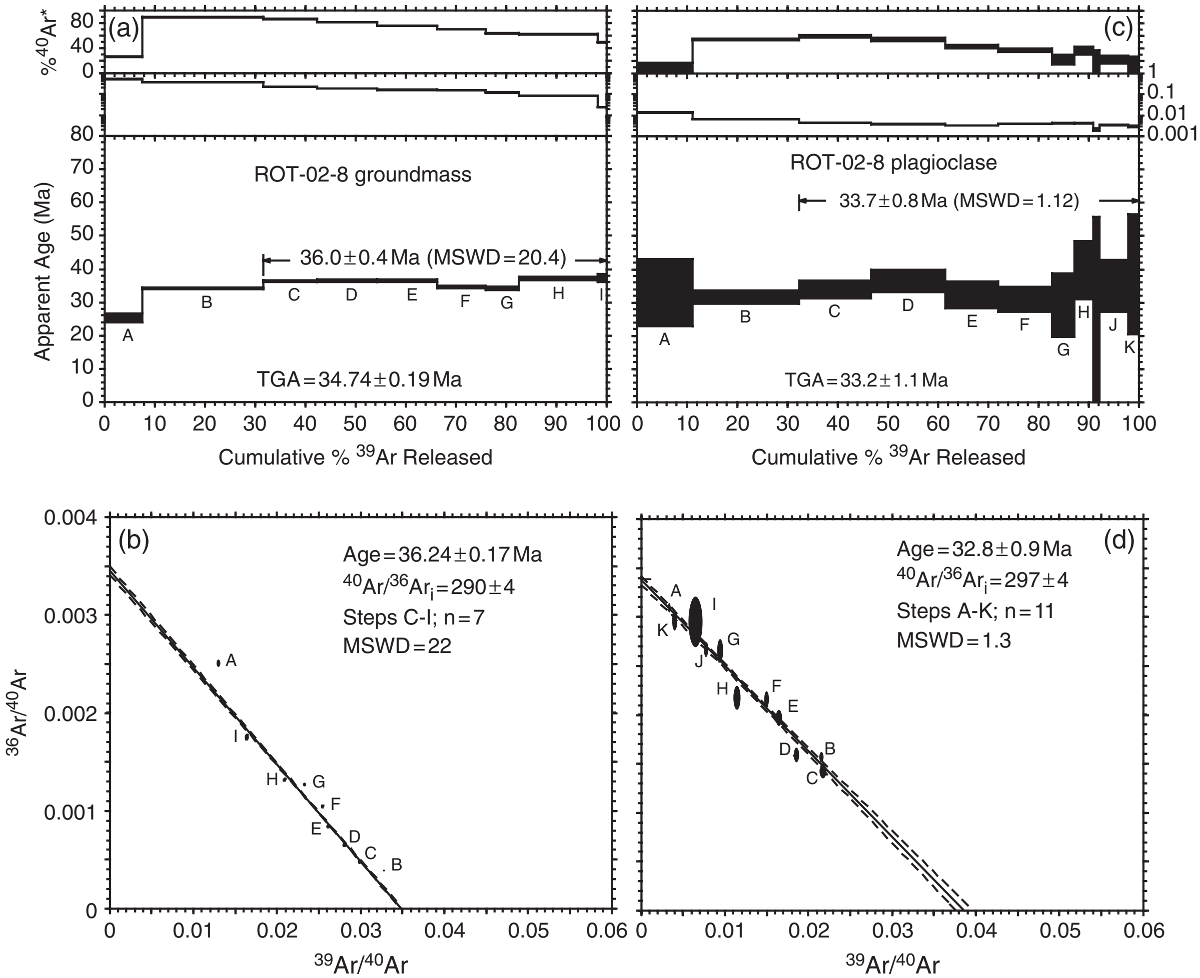

Fig. 4. $^{40}Ar/^{39}Ar$ age spectra (a, c) and isotope correlation diagrams (b, d) for groundmass and plagioclase for sample ROT02-8.

age ($32{\cdot}4 \pm 0{\cdot}9$ Ma) that is within error of the coexisting groundmass concentrate ($34{\cdot}8 \pm 0{\cdot}4$ Ma). Although the plagioclase weighted mean ages have lower MSWD values compared with their groundmass pairs, the significant corrections for irradiation-derived ^{36}Ar and ^{39}Ar from Ca interference, coupled with high blank corrections related to small argon signals, cause these plagioclases to have potentially high systematic errors. Thus, the groundmass concentrates are considered to provide the most accurate eruption ages for the Rota samples.

A hornblende separate from an andesite (Gum 80-1b) from near the base of the Alutom Formation on Guam (see Reagan & Meijer, 1984) yields a well-behaved spectrum with a plateau age of $38{\cdot}3 \pm 0{\cdot}6$ Ma for more than 90% of the ^{39}Ar released (Fig. 5a). Although the age spectrum is poorly resolved, the plateau age has an acceptable MSWD of 0·9 and is concordant with the isochron age (Fig. 5b, Table 1), and is therefore interpreted to yield a reliable date for early first-arc volcanism in this part of the IBM system.

WHOLE-ROCK GEOCHEMISTRY

Major elements

The rhyolites of the proto-arc Sankakuyama Formation on Saipan can be subdivided into those found on Mount Achuago with 79–81 wt % SiO_2 and those found on the coast near Bird Island with 77–78 wt % SiO_2 (Table 2). The Bird Island rhyolites have higher concentrations of Al_2O_3 (12·6–12·7 wt %), Fe_2O_3 (1·5–1·6 wt %), and K_2O (2·5–3·0 wt %) compared with those from Mount Achuago (Al_2O_3 10·5–11·3 wt %; Fe_2O_3 1·25–1·45 wt %; K_2O 1·30–1·35 wt %; Fig. 6a, b and f). Because the stony rhyolites from Mount Achuago contain secondary quartz, the extreme SiO_2 concentrations and low concentrations of most other major elements compared with the glassy rhyolites from the Bird Island area are largely attributed to alteration and silicification. Nevertheless, the K_2O concentrations of the Bird Island and Mount Achuago rhyolites consistently differ by a factor of two, indicating that they represent separate medium- and low-K lineages. The high

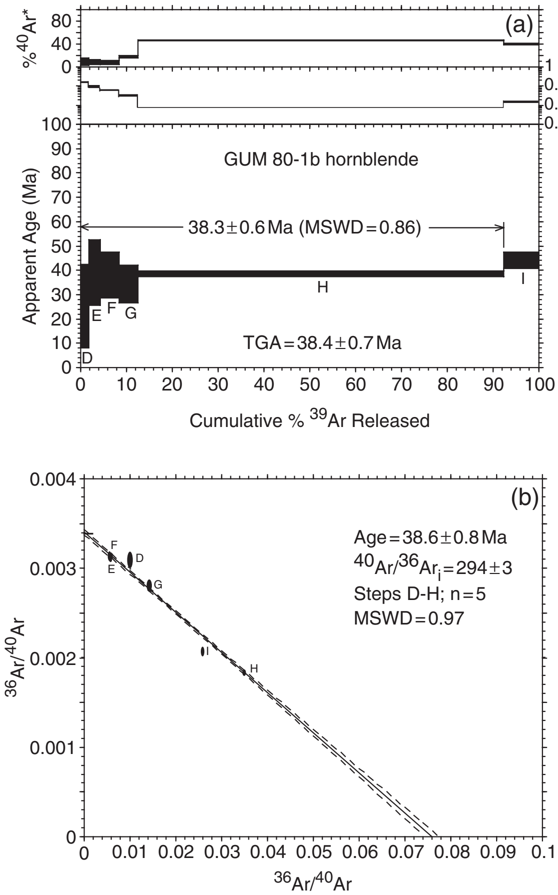

Fig. 5. $^{40}Ar/^{39}Ar$ age spectrum (a) and isotope correlation diagram (b) for hornblende from sample GUM80-1b. This sample was also dated by K–Ar methods (Meijer *et al.*, 1983). Its major and trace element compositions have been reported by Reagan & Meijer (1984).

normative quartz content of the rhyolites from Saipan (normalized CIPW weight norm for SPN02-12: Q = 45·6; Ab = 35·0; Or = 17·6) indicates that final crystallization occurred at pressures of 100 MPa or less (see Blundy & Cashman, 2001).

Most lavas from the Ogo volcanics on Rota and the Hagman Formation on Saipan are low-K silicic andesites and dacites (see Gill, 1981). The concentrations of major elements in these lavas are relatively diverse at a given SiO_2 concentration. For example, Al_2O_3 concentrations range from 17·1 to 21·6 wt %, Fe_2O_3* from 4·4 to 7·2 wt %, and K_2O from 0·5 to 1·0 wt % at *c.* 61 wt % SiO_2 (Table 2; Fig. 6a, b and f). Samples of the Sabana andesite on Rota are high-Mg basaltic andesites with 56 wt % SiO_2, 18 wt % Al_2O_3, 4·9 wt % MgO, FeO*/MgO = 1·26, and 0·5 wt % TiO_2 (Figs 6a, c, e and 7).

Trace elements

The first-arc silicic andesites and dacites from the Hagman Fm. and the Ogo volcanics have incompatible trace element patterns that are similar to those reported for first-arc volcanic rocks from throughout the IBM system (e.g. Hickey-Vargas & Reagan, 1987; Gill *et al.*, 1994; Ishizuka *et al.*, 2006), including relatively flat REE patterns (normalized La/Yb = 0·7–1·6), significant depletions in Nb and Ta, and enrichments in the large ion lithophile elements (LILE) relative to the light REE (LREE) (Fig. 8). The Sabana andesite from Rota differs from these more differentiated lavas by having higher concentrations of light Sr, REE, Pb, and Th, but significantly lower concentrations of the high field strength elements (HFSE) Nb, Ta, Zr, and Hf (Fig. 8).

Many first-arc samples have negative Ce anomalies, including some that are significantly deeper than those observed for modern Mariana arc lavas (Saipan and Rota first-arc Ce/Ce* = 0·66–1·04: Fig. 8; modern arc Ce/Ce* = 0·94–0·99; Elliott *et al.*, 1997). For the modern arc, similar anomalies have been explained by recycling REE from subducted sediments with negative Ce anomalies (Elliott *et al.*, 1997). However, large Ce anomalies in other incipiently to moderately altered arc rocks have been explained by preferential mobilization of trivalent REE over tetravalent Ce in oxidized and acidic groundwaters during weathering to produce soils (Patino *et al.*, 2003). Because the first-arc rocks analyzed here all show evidence of groundmass alteration and the depths of the Ce anomalies in the first-arc rocks are highly variable and do not correlate with other trace element or isotopic measures of the influence of subducted components in magma genesis, we attribute these anomalies to weathering rather than to any petrogenetic process.

The primitive mantle normalized incompatible trace element patterns for the proto-arc rhyolites from the Sankakuyama Fm. on Saipan (Fig. 9) are transitional between those of the local first-arc lavas and proto-arc lavas from other locations in the IBM system. For example, ratios between LILE and REE (e.g. Rb/La; Fig. 10b) in the rhyolites are higher than those of first-arc or later lavas, but lower than the highest values found in proto-arc lavas such as the boninites from DSDP Site 458 and Chichijima. The trace element characteristics of the rhyolites that are most similar to those of the first-arc andesites and dacites are the relatively low REE concentrations (Table 2) and flat REE patterns (normalized La/Yb = 0·8–1·3; Fig. 9).

La/Nb ratios are higher for the rhyolites than for all but a few other Mariana proto-arc lavas, but overlap with the lower values measured for first-arc and later lavas (Fig. 10a). This ratio is one of the most diagnostic of arc volcanism in general (e.g. Gill, 1981; Reagan & Gill, 1989), and the low La/Nb values of boninitic proto-arc lavas are one of the key indicators that melting conditions or processes were different in the proto-arc than during more 'normal' subduction that came later. Nevertheless, the relatively high value for this ratio in the rhyolites suggests that the normal arc trace element signal appeared

Table 2: Major and trace element abundanes in wt % and μg/g, respectively

	Proto-arc						
	Saipan: Sankakuyama Formation						Guam: Facpi Fm.
Sample:	SPN02-1	SPN02-2	SPN02-4	SPN02-11	SPN02-12	SPN02-13	GUM02-40
SiO_2	81·43	80·91	77·29	76·90	77·31	79·83	56·95
TiO_2	0·09	0·09	0·10	0·10	0·10	0·09	0·56
Al_2O_3	10·59	10·91	12·62	12·69	12·71	11·26	14·69
$Fe_2O_3^*$	1·40	1·45	1·54	1·56	1·60	1·27	9·03
MnO	0·04	0·04	0·08	0·07	0·08	0·01	0·14
MgO	0·03	0·00	0·03	0·08	0·03	0·04	6·54
CaO	0·86	0·83	0·97	0·98	0·93	0·88	8·77
Na_2O	4·10	4·30	4·30	3·83	3·75	4·43	2·56
K_2O	1·30	1·35	2·55	3·04	2·98	1·36	0·77
P_2O_5	0·04	0·03	0·03	0·05	0·05	0·02	0·09
Total	99·87	99·91	99·51	99·29	99·54	99·18	100·09
LOI	1·01	0·98	4·30	4·74	4·95	0·89	3·43
Li	5·29	4·11	3·85	3·34	2·59	9·96	9·91
Be	0·76	0·71	1·00	0·90	0·98	0·72	0·73
Cs	0·48	0·48	0·92	0·91	0·92	0·19	0·43
Rb	20·1	19·2	28·4	27·1	29·1	13·1	13·7
Ba	127	131	137	133	133	158	80
Sr	67	62	72	69	68	68	134
Pb	3·35	3·43	4·40	4·00	4·26	3·78	2·07
Th	0·42	0·43	0·54	0·56	0·56	0·43	0·67
U	0·44	0·51	0·48	0·46	0·47	0·46	0·35
Nb	0·87	0·81	1·04	0·96	1·04	0·84	2·95
Ta	0·07	0·08	0·10	0·09	0·10	0·08	0·20
La	4·20	4·62	4·85	4·74	4·84	4·87	4·32
Ce	10·9	11·1	13·6	11·6	13·0	11·4	9·7
Pr	1·70	1·89	1·98	1·88	1·98	2·11	1·20
Nd	8·31	9·30	10·12	9·38	9·79	10·35	5·49
Zr	85·0	88·6	114·6	109·3	117·0	96·6	52·7
Hf	2·50	2·79	3·32	3·39	3·38	3·00	1·58
Sm	2·61	3·00	3·35	3·17	3·21	3·33	1·67
Eu	0·56	0·56	0·64	0·60	0·59	0·64	0·56
Gd	3·33	3·70	4·47	4·31	4·36	3·63	2·22
Tb	0·58	0·66	0·81	0·78	0·79	0·63	0·40
Dy	3·88	4·24	5·44	5·26	5·40	3·90	2·66
Ho	0·86	0·93	1·22	1·19	1·22	0·85	0·59
Er	2·54	2·80	3·72	3·59	3·69	2·51	1·74
Yb	2·79	3·08	4·14	4·01	4·13	2·77	1·85
Lu	0·46	0·50	0·68	0·66	0·67	0·44	0·30
Y	27·2	28·8	39·7	38·5	40·1	25·0	16·7
V	2·6	1·0	0·2	0·2	0·3	0·8	239·9
Sc	11·9	12·8	14·5	14·2	14·4	12·7	30·6
Ni	0·7	b.d.	0·7	b.d.	1·2	b.d.	93·2
Cr	1·6	0·3	1·2	0·6	1·5	0·2	256·1
Co	1·0	0·1	1·2	0·5	1·1	0·8	29·2
Cu	2·0	1·4	2·4	1·9	2·5	1·7	98·9
Zn	35·6	34·9	50·9	51·1	51·4	28·5	65·0
Ga	13·1	13·6	15·1	14·8	15·2	14·7	14·5
As	0·45	0·82	1·36	1·32	1·28	0·63	0·98

(continued)

Table 2: Continued

	First-arc							
	Saipan: Hagman Formation					Guam: Facpi and Alutom Fms.		
Sample:	SPN02-6	SPN02-7	SPN02-8-B	SPN02-9	SPN02-10	GUM80-94	NIM80-2	GUM02-7
SiO_2	58·43	65·83	61·31	60·59	59·55	53·37	50·17	72·80
TiO_2	0·58	0·41	0·40	0·57	0·56	0·43	0·50	0·29
Al_2O_3	18·03	19·05	21·57	19·61	18·14	17·90	18·06	14·16
Fe_2O_3*	8·06	2·85	4·38	4·64	6·63	8·43	8·55	3·07
MnO	0·14	0·04	0·10	0·05	0·08	0·13	0·14	0·03
MgO	3·65	0·29	1·36	1·72	2·73	8·21	9·09	0·96
CaO	8·46	7·19	6·80	8·38	8·17	10·09	11·57	3·88
Na_2O	2·56	3·44	3·06	2·95	2·70	1·97	1·78	3·68
K_2O	0·35	0·72	0·46	0·98	0·96	0·15	0·18	0·97
P_2O_5	0·11	0·12	0·09	0·12	0·12	0·06	0·06	0·11
Total	100·37	99·94	99·54	99·63	99·63	100·74	100·10	99·93
LOI	0·72	0·64	4·87	0·86	0·74	1·37	2·16	0·89
Li	5·78	7·76	12·27	10·72	13·09	8·39	8·06	10·34
Be	0·33	0·45	0·39	0·42	0·41	0·35	0·32	0·82
Cs	0·35	0·43	0·47	0·24	0·41	0·03	0·11	0·26
Rb	4·8	11·3	8·5	18·1	19·2	1·2	2·4	15·1
Ba	83	120	180	131	121	19	48	99
Sr	188	205	281	211	193	139	149	153
Pb	2·36	2·86	2·31	2·77	4·83	1·53	0·99	1·91
Th	0·26	0·24	0·20	0·64	0·62	0·12	0·20	0·36
U	0·14	0·18	0·13	0·95	0·37	0·10	0·10	0·23
Nb	0·45	0·65	0·55	0·56	0·49	0·39	0·52	1·37
Ta	0·05	0·06	0·06	0·05	0·05	0·04	0·05	0·10
La	2·81	3·63	3·11	4·01	4·64	1·38	2·42	5·20
Ce	8·0	10·0	8·1	11·3	11·3	3·8	6·7	11·7
Pr	1·28	1·63	1·33	1·68	1·82	0·68	1·07	1·82
Nd	6·95	8·47	6·92	8·37	9·37	3·54	5·32	8·45
Zr	68·5	61·3	56·3	86·7	79·9	28·2	42·1	63·9
Hf	2·04	1·94	1·81	2·53	2·46	0·88	1·16	1·87
Sm	2·45	2·78	2·29	2·58	2·98	1·21	1·69	2·50
Eu	0·76	0·87	0·82	0·77	0·84	0·47	0·64	0·73
Gd	3·42	3·71	3·37	3·19	4·08	1·73	2·21	3·11
Tb	0·61	0·65	0·61	0·55	0·70	0·32	0·39	0·54
Dy	4·12	4·32	4·27	3·50	4·54	2·08	2·53	3·45
Ho	0·91	0·93	0·98	0·74	1·00	0·47	0·57	0·75
Er	2·65	2·67	2·94	2·04	2·86	1·37	1·63	2·17
Yb	2·76	2·61	3·08	1·90	2·95	1·48	1·62	2·18
Lu	0·44	0·40	0·49	0·29	0·47	0·25	0·25	0·35
Y	24·8	26·9	30·9	22·0	29·4	14·0	16·4	22·1
V	215·2	48·2	85·3	184·3	190·2	217·3	235·3	23·1
Sc	30·0	11·9	17·8	28·1	27·3	33·7	39·6	8·6
Ni	9·3	2·7	3·6	13·2	12·5	152·5	102·1	41·4
Cr	23·4	2·6	4·3	22·7	24·2	311·0	372·3	2·6
Co	22·0	5·2	9·0	14·7	21·3	37·8	36·1	6·8
Cu	48·1	23·5	62·2	76·6	22·5	90·3	99·9	5·8
Zn	72·2	99·2	41·7	61·5	64·3	73·8	63·0	34·6
Ga	15·4	16·6	17·6	17·3	15·4	14·0	14·8	15·3
As	0·83	1·13	1·40	0·94	0·99	0·83	0·56	0·83

(continued)

Table 2: Continued

	First-arc						
	Rota: Ogo volcanics					Rota: Sabana andesite	
Sample:	ROT02-1	ROT02-2	ROT02-3-B	ROT02-5	ROT02-6	ROT02-7	ROT02-8
SiO_2	64·08	64·03	60·61	62·62	57·81	56·28	56·39
TiO_2	0·65	0·65	0·54	0·58	0·58	0·50	0·50
Al_2O_3	15·60	15·56	17·58	17·05	18·05	18·24	18·19
$Fe_2O_3^*$	7·25	7·23	7·24	6·50	8·17	6·91	6·91
MnO	0·11	0·11	0·13	0·10	0·13	0·11	0·11
MgO	1·59	1·66	2·19	1·68	3·02	4·93	4·88
CaO	5·55	5·58	7·60	6·07	8·38	9·21	9·24
Na_2O	3·79	3·72	3·15	3·80	2·92	2·33	2·45
K_2O	1·03	1·02	0·76	1·06	0·82	1·21	1·06
P_2O_5	0·14	0·15	0·10	0·12	0·12	0·13	0·13
Total	99·79	99·71	99·89	99·59	100·01	99·86	99·86
LOI	0·66	0·77	0·84	0·42	0·08	1·05	4·87
Li	8·61	8·56	8·10	10·51	8·31	3·83	3·86
Be	0·92	0·84	0·69	0·86	0·68	0·66	0·65
Cs	0·49	0·48	0·39	0·15	0·14	0·12	0·10
Rb	17·7	17·3	11·6	16·3	12·8	6·2	5·7
Ba	138	133	99	130	99	134	126
Sr	141	140	151	163	162	549	538
Pb	3·16	3·08	2·29	2·56	2·08	2·82	2·88
Th	0·77	0·74	0·42	0·58	0·43	1·64	1·64
U	0·42	0·46	0·25	0·32	0·25	0·62	0·47
Nb	1·23	1·19	0·79	1·14	0·83	0·52	0·51
Ta	0·11	0·10	0·07	0·09	0·07	0·04	0·05
La	8·39	6·24	3·99	6·17	4·50	6·65	6·65
Ce	12·9	11·8	9·5	11·4	9·0	13·7	13·7
Pr	2·64	1·98	1·39	1·83	1·43	2·06	2·39
Nd	12·84	9·64	6·96	9·18	7·06	9·72	11·34
Zr	93·9	92·9	55·1	78·8	52·6	49·3	49·2
Hf	2·82	2·72	1·78	2·17	1·61	1·56	1·57
Sm	3·87	2·92	2·28	2·73	2·18	2·51	3·12
Eu	1·13	0·90	0·77	0·91	0·77	0·90	1·09
Gd	5·38	4·02	3·17	4·00	3·16	3·08	3·69
Tb	0·91	0·69	0·56	0·67	0·53	0·47	0·60
Dy	5·90	4·52	3·71	4·44	3·53	2·89	3·74
Ho	1·33	1·02	0·84	1·02	0·81	0·65	0·82
Er	3·85	2·98	2·46	3·06	2·35	1·89	2·41
Yb	3·84	3·06	2·61	2·95	2·35	1·73	2·41
Lu	0·63	0·50	0·42	0·49	0·39	0·28	0·39
Y	43·1	32·8	25·0	39·4	25·7	24·1	25·3
V	175·4	168·8	181·6	140·9	247·7	228·1	225·3
Sc	22·1	21·3	25·3	22·6	30·0	26·6	26·6
Ni	0·6	3·1	3·9	12·2	12·7	33·1	32·4
Cr	3·7	3·5	29·4	17·7	20·1	57·4	55·6
Co	15·7	15·2	16·7	13·3	19·3	22·9	22·9
Cu	68·3	81·8	96·6	16·7	32·5	72·3	79·8
Zn	74·4	74·6	70·5	63·0	68·7	55·4	54·9
Ga	17·0	16·5	16·3	17·9	17·3	18·8	18·8
As	1·04	0·98	0·83	0·53	0·61	0·52	0·45

b.d., Below detection limit; LOI, loss on ignition. Sample locations are given in Electronic Appendix 2.

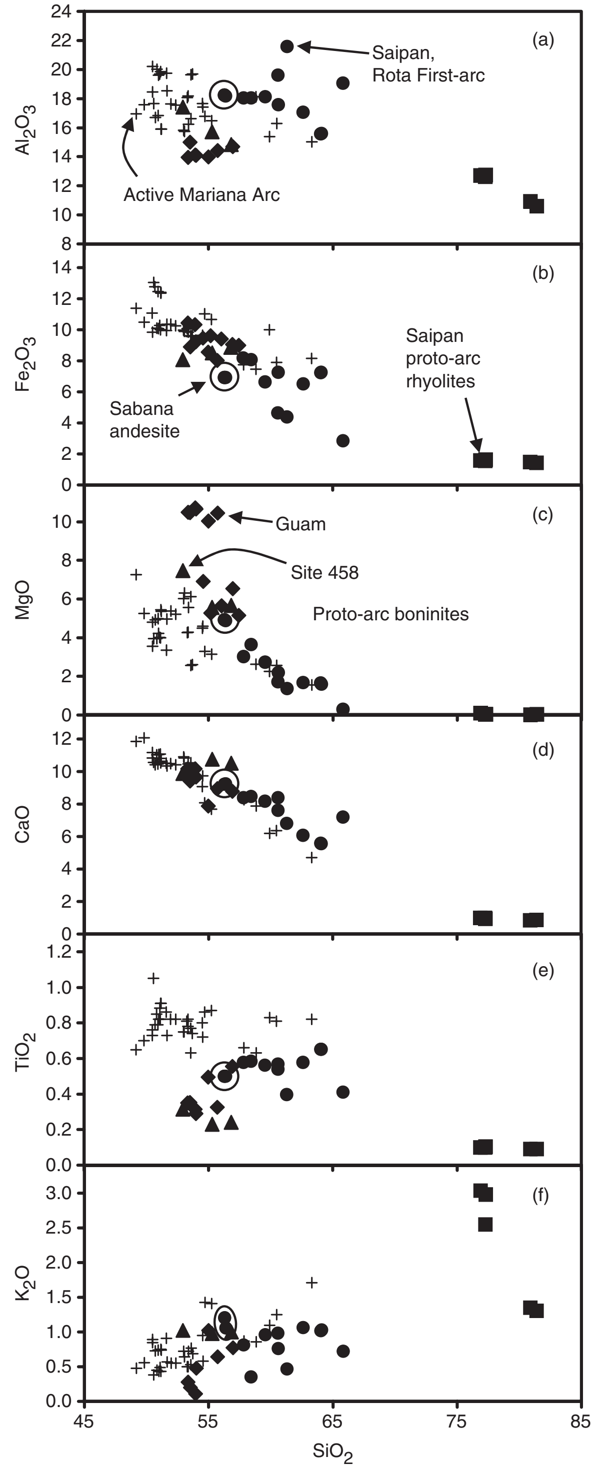

Fig. 6. Variation of major element oxide concentrations with SiO_2. All data are in wt %. •, whole-rock analyses from first-arc andesites from Saipan and Rota; ■, proto-arc rhyolites from Saipan; ◆, whole-rock analyses of boninites from the proto-arc Facpi formation on Guam; ▲, analyses of boninites from DSDP Site 458 (Table 2; Reagan & Meijer (1984); Pearce *et al.*, 1999); +, whole-rock analyses from the modern arc (Elliott *et al.*, 1997; Woodhead *et al.*, 2001). The analyses of the Sabana andesite are circled.

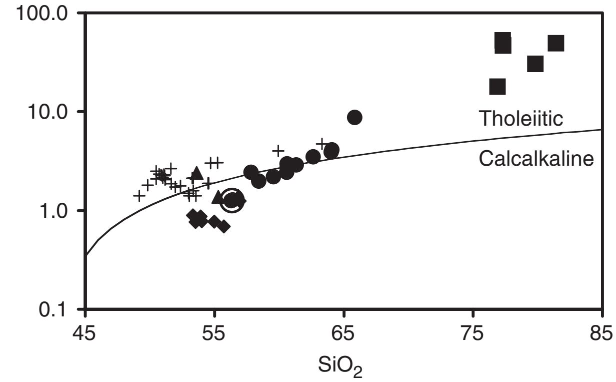

Fig. 7. Semi-logarithmic plot of FeO*/MgO vs wt % SiO_2. Division between tholeiite and calc-alkaline series samples after Miyashiro (1974). A logarithmic scale is used for FeO*/MgO to accommodate the extreme values of the Saipan rhyolites. Symbols are the same as for Fig. 6.

in lavas erupted at Saipan before other locations in the IBM system.

Radiogenic isotopes

The initial $^{87}Sr/^{86}Sr$ and $^{143}Nd/^{144}Nd$ compositions of the proto-arc and first-arc samples from Saipan and Rota (Table 3) are similar to those of other proto-arc and first-arc Mariana samples (Fig. 11). Sr isotopic compositions are more radiogenic than those of mid-ocean ridge basalt (MORB) or Philippine Basin lavas (Hickey-Vargas, 1991), whereas Nd isotopic compositions overlap for lavas from all of these settings. Similar observations for volcanic arcs globally have been explained by the transfer of Sr but not Nd from the subducting plate in a water-rich fluid to the mantle sources of the parental magmas to the lavas (e.g. DePaolo & Wasserburg, 1977; Carr *et al.*, 1990). The Sabana andesite has more radiogenic Nd and less radiogenic Sr than other first-arc samples.

On a plot of Hf against Nd isotopes (Fig. 12), the proto-arc and first-arc samples from Saipan and Rota plot in the Indian Ocean MORB field (see Pearce *et al.*, 1999; Chauvel & Blichert-Toft, 2001; Kempton *et al.*, 2002; Hanan *et al.*, 2004; Graham *et al.*, 2006). The Sabana andesite is again the exception, plotting within the overlapping area of the Pacific and Indian MORB fields because of its higher $^{143}Nd/^{144}Nd$ value compared with other first-arc rocks.

The least radiogenic Pb isotope compositions of the lavas studied here are those of the Sabana andesite samples (Table 3). On a plot of $^{208}Pb/^{204}Pb$ against $^{206}Pb/^{204}Pb$ (Fig. 13a), these samples plot near the Pb isotope values measured for high-Mg basaltic andesites drilled at ODP Site 793b (Taylor *et al.*, 1992), which underlie basin sediments in the fore-arc east of the Izu arc. The Sabana andesites fall on the Pacific side of the dividing line drawn between Pacific and Indian MORB by Pearce *et al.* (1999). On this plot, as well as that of $^{208}Pb/^{204}Pb$ against

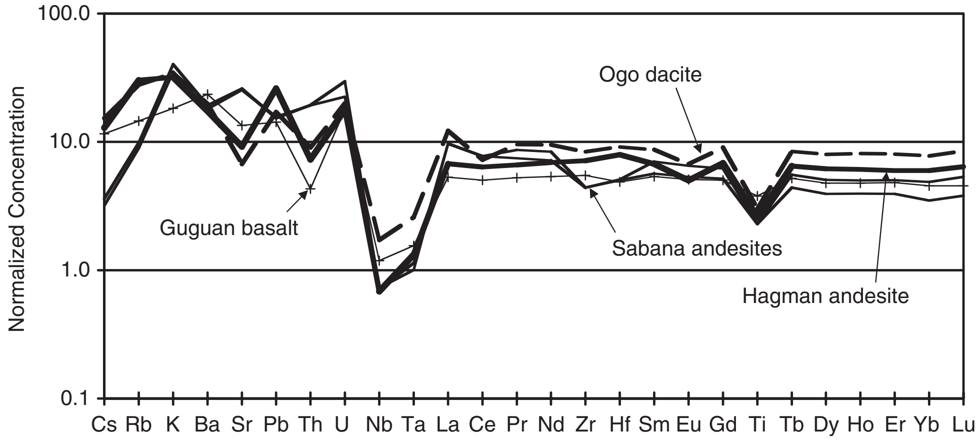

Fig. 8. Primitive mantle-normalized (Sun & McDonough, 1989) incompatible trace element patterns for first-arc lavas from Rota (Ogo dacite ROT02-1, thick dashed line) and Sabana andesites (ROT02-7 and ROT02-8, intermediate continuous lines) and Saipan (Hagman Fm. andesite SPN02-10, thick solid line). Data are from Table 2. Also shown is an active arc basalt from Guguan (GU-6; Woodhead *et al.*, 2001; thin line with plus symbols). Elements are arranged by group and degree of incompatibility. Elements considered to have high concentrations in fluids from subducting lithosphere (large-ion lithophile elements and the U-group elements U, Th, and Pb) are to the left. Less soluble REE and HFSE are to the right. Incompatibility during melting generally decreases to the right.

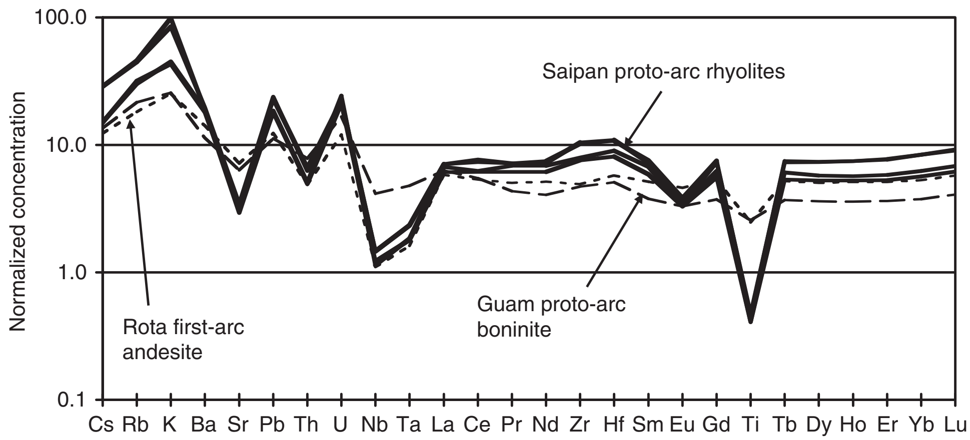

Fig. 9. Primitive mantle-normalized incompatible trace element patterns for proto-arc rhyolites from Saipan (continuous lines) and a representative first-arc lava (ROT02-3) from the Ogo volcanics on Rota (short dashed line). The trace element composition of a 44 Ma boninite (GUM02-40) from Guam (long dashed line) is shown for comparison. Data are from Table 2.

$^{207}Pb/^{204}Pb$ (Fig. 13b), these samples mark the least radiogenic ends of trends for proto-arc, first-arc, and modern Mariana arc lavas, suggesting that this unradiogenic endmember is widespread and has persisted throughout the duration of the arc. The proto-arc rhyolites, first-arc andesites and dacites, and modern Mariana arc lavas plot between the Sabana andesite and silicic sediments such as Jurassic and younger cherty and clay-rich sediments (Meijer, 1976; Ben Othman *et al.*, 1989), including Cenozoic sediments rich in aeolian dust from Asia (Pettke *et al.*, 2000). In contrast, proto-arc volcanic rocks from Guam and DSDP Sites 458 and 459 have Pb isotope compositions that plot between the Sabana andesite and ocean island basalt (OIB) from the Magellan Seamounts in the western Pacific and associated volcaniclastic sediments, which are characterized by radiogenic $^{206}Pb/^{204}Pb$ (Hickey-Vargas & Reagan, 1987; Smith *et al.*, 1989; Staudigel *et al.*, 1991; Elliott *et al.*, 1997; Pearce *et al.*, 1999; Woodhead *et al.*, 2001).

WEBSTERITE XENOLITHS

Representative major element compositions for adjacent clinopyroxene and orthopyroxene rims in websterite xenoliths from the Sabana andesite are illustrated in Table 4. The clinopyroxenes are augites with En = 45–48, Fs = 8–15, and Wo = 40–46. Orthopyroxenes have compositions restricted to En = 78–79, Fs = 20–22, and Wo = 3–4.

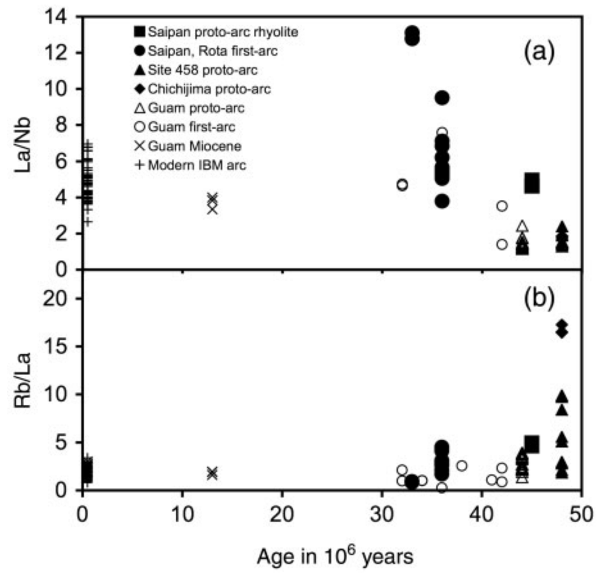

Fig. 10. La/Nb (a) and Rb/La (b) vs age of eruption for volcanic rocks from the IBM system and fore-arc. Ages are based on dating presented here and by Meijer *et al.* (1983) and Cosca *et al.* (1998). Data are from Table 1 and the literature (Reagan & Meijer, 1984; Hickey-Vargas & Reagan, 1987; Taylor *et al.*, 1992; Elliott *et al.*, 1997; Pearce *et al.*, 1999; Woodhead *et al.*, 2001; Mohler, 2003; Ishizuka *et al.*, 2006).

Geothermometry estimates using rims on adjacent pyroxenes in the xenoliths gave a restricted temperature range of 1050–1090°C using two-pyroxene geothermometery (QUIlF; Anderson *et al.*, 1993). Assuming a temperature of 1070°C, the Al-in-clinopyroxene geobarometer for hydrous melts of Nimis & Ulmer (1998) and Nimis (1999) gives pressures of 0·24–0·44 GPa (Table 4). These data suggest that the websterite xenoliths are cumulates from the middle crust, and not sub-crustal assemblages.

DISCUSSION

Petrogenesis of proto-arc rhyolites

The rhyolites from the Sankakuyama Fm. of Saipan erupted at 45·1 ±0·3 Ma, during the period of boninite-dominated volcanism in the Mariana arc recorded at DSDP Sites 458 and 459, Palau, the Bonin Ridge and Guam (48–44 Ma; Meijer *et al.*, 1983; Cosca *et al.*, 1998; Reagan *et al.*, 2003; Ishizuka *et al.*, 2006). However, the relatively flat REE patterns and high La/Nb values of the rhyolites (Figs 9 and 10) indicate that the HFSE and REE concentrations reflect sources and/or magma generation processes that have more in common with those of the first-arc and later IBM lavas than with the proto-arc boninites (see Meijer, 1983). Therefore, the principal question that needs to be addressed is why were high-Si rhyolites with relatively normal arc trace element patterns generated so early in the IBM system history beneath Saipan?

One of the most interesting features of the IBM system is the significant abundance of silicic magmas that have erupted throughout its history (e.g. Bryant *et al.*, 1999; Straub, 2003). Another is the dominance of low P-wave velocities (6·0–6·5 km/s) in the middle crust of the IBM system and fore-arc, which has been interpreted as tonalitic to granitic intrusions (Suyehiro *et al.*, 1996; Takahashi *et al.*, 1998, 2007; Kitamura *et al.*, 2003; Calvert *et al.*, 2005). It is likely that these two observations are related, as the presence of crust with a relatively low density is considered necessary to generate large volumes of rhyolite by differentiation of more mafic magmas (e.g. Glazner & Ussler, 1989). Indeed, the initial production of such crust as a result of crystal fractionation of more mafic magmas or melting of arc crust (e.g. Tamura & Tatsumi, 2002) could become self-perpetuating, and lead to the relatively thick sections of middle crust seen in the modern IBM system. Kodaira *et al.* (2007) showed that voluminous rhyolitic volcanism occurs only in the Izu section of the Izu–Bonin arc, where the average crust is relatively thick. However, rhyolitic volcanic centers overlie areas with middle crust ($V_p = 6{\cdot}0$–$6{\cdot}8$) that is thinner than that beneath nearby mafic volcanic centers. One explanation for this counter-intuitive observation is that the rhyolites represent the low melting fraction that was distilled from the tonalitic middle crust and erupted. If so, then the 45 Ma rhyolites on Saipan may represent the distillates of early tonalitic crust in the Mariana fore-arc.

Significant thicknesses of silicic crust probably did not exist in the regions erupting boninites during the middle Eocene. These regions have commonly been thought to represent *in situ* 'arc ophiolites' (Bloomer & Hawkins, 1983) consisting of thin and undifferentiated crust that was generated in an extensional fore-arc setting (Reagan & Meijer, 1984; Stern & Bloomer, 1992). The appearance of tonalitic to granitic crust and the onset of rhyolitic volcanism in the IBM system may have occurred in areas that had ceased extending and had begun to differentiate internally.

Based on this reasoning, we contend that Saipan was built on boninitic crust that was generated during an episode of massive fore-arc extension at around 48 Ma (see Stern & Bloomer, 1992; Stern *et al.*, 2003; Ishizuka *et al.*, 2006). Instead of undergoing continued extension as on Guam (see Reagan & Meijer, 1984), however, the crust beneath Saipan ceased extending at about 45–46 Ma and became compositionally differentiated to the point at which it could produce high-Si rhyolite. If this model is correct, then crust stabilization and normal arc magmatism both began 3–4 Myr earlier beneath Saipan than elsewhere in the Mariana arc, and about 1 Myr before the first lavas with normal arc-like trace element signatures in the Izu–Bonin system (Ishizuka *et al.*, 2006).

Table 3: Isotopic compositions of selected samples

Sample	$^{87}Sr/^{86}Sr$	$^{87}Sr/^{86}Sr^{\circ}$	$^{143}Nd/^{144}Nd$	$^{143}Nd/^{144}Nd^{\circ}$	$^{176}Hf/^{177}Hf$	$^{176}Hf/^{177}Hf^{\circ}$	$^{208}Pb/^{204}Pb$	$^{207}Pb/^{204}Pb$	$^{206}Pb/^{204}Pb$
Saipan: proto-arc									
SPN 02-4	0·704247	0·703520	0·513045	0·512986	0·283238	0·283213	38·086	15·521	18·413
SPN 02-11	0·704318	0·703594	0·513045	0·512985	0·283226	0·283202	38·047	15·506	18·397
SPN 02-12	0·704373	0·703579	0·513052	0·512982	0·283231	0·283207	38·000	15·497	18·372
Guam: proto-arc									
GUM02-40	0·704168	0·703984	0·512983	0·512930	0·283139	0·283116			
Saipan: first-arc									
SPN 02-6	0·703614	0·703577			0·283255	0·283234	38·202	15·512	18·406
SPN 02-7	0·703587	0·703505	0·513061	0·513014	0·283244	0·283224	38·243	15·525	18·425
Guam: first-arc									
GUM80-94	0·703569	0·703554	0·513080	0·513023	0·283234	0·283202	38·160	15·523	18·500
NIM80-2	0·703211	0·703189	0·513038	0·512998	0·283219	0·283200	37·953	15·484	18·353
GUM02-7	0·704105	0·703959	0·513048	0·513006	0·283213	0·283194	38·278	15·560	18·548
Rota: first-arc (Ogo)									
ROT 02-1	0·703677	0·703492	0·513049	0·513006	0·283221	0·283199	38·108	15·501	18·496
ROT 02-3	0·703663	0·703536	0·513049	0·513002	0·283232	0·283209	38·143	15·513	18·486
Rota: first-arc (Sabana)									
ROT 02-7	0·703031	0·703014			0·283218	0·283200	37·850	15·447	18·301
ROT 02-7(dup)							37·852	15·447	18·301
ROT 02-8	0·703086	0·703070	0·513092	0·513053	0·283214	0·283189	37·858	15·448	18·292

The $^{87}Sr/^{86}Sr$ is reported relative to the NIST SRM 987 value of 0·71025, $^{143}Nd/^{144}Nd$ relative to the La Jolla Nd value of 0·511844, $^{176}Hf/^{177}Hf$ relative to the JMC 475 value of 0·282160, $^{206}Pb/^{204}Pb$, $^{207}Pb/^{204}Pb$, and $^{208}Pb/^{204}Pb$ relative to the values reported for NIST NBS 981 by Todt *et al*. (1996). The small 'o' superscript indicates initial values.

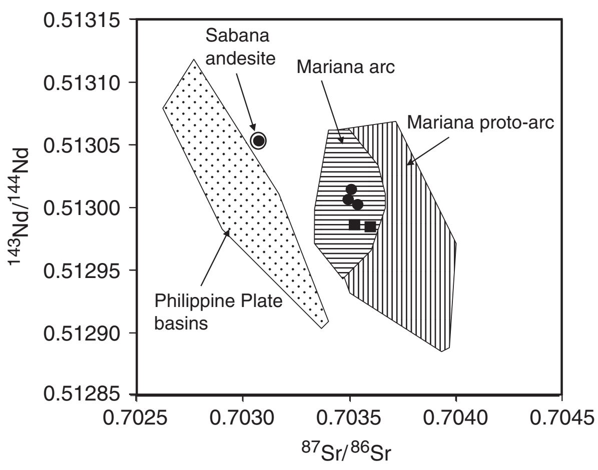

Fig. 11. Age-corrected $^{143}Nd/^{144}Nd$ vs $^{87}Sr/^{86}Sr$. ●, first-arc lavas from Saipan and Rota (age-corrected to 36 Ma); ■, proto-arc rhyolites from Saipan (corrected to 45 Ma). The Sabana andesite is circled. These data are compared with the equivalent data from the Philippine plate basins (stippled field; Hickey-Vargas, 1991; Pearce *et al.*, 1999), modern arc (horizontally ruled field; Elliott *et al.*, 1997; Woodhead *et al.*, 2001), and Mariana proto-arc (vertically ruled field; Hickey-Vargas & Reagan, 1987; Pearce *et al.*, 1999; Reagan *et al.*, 2003).

An alternative explanation for the difference in the style of volcanism between Saipan and other proto-arc areas is that Saipan might be underlain by a remnant of older crust, perhaps of Cretaceous or Paleocene age, such as the Daito and Oki Daito Ridges, and Amami Plateau along the northern margin of the West Philippine Basin (Honza & Fujioka, 2004). However, we do not favor this explanation because Saipan's rhyolites have isotopic, REE and HFSE characteristics that have affinities with IBM first-arc magmas, whereas the Cretaceous arc lavas on the Amami Plateau have much steeper REE patterns and significantly less radiogenic Sr isotopic compositions (see Hickey-Vargas, 2005).

The high-Si rhyolites on Saipan have near-eutectic compositions, and this feature precludes quantitative modeling of the process that led to their final major element compositions. Trace elements, however, can be modeled because Henry's Law governs their partitioning between melts and crystalline phases. As noted above, the rhyolites from Saipan have incompatible trace element and isotopic characteristics that are intermediate between those of proto-arc boninites and first-arc intermediate to silicic lavas.

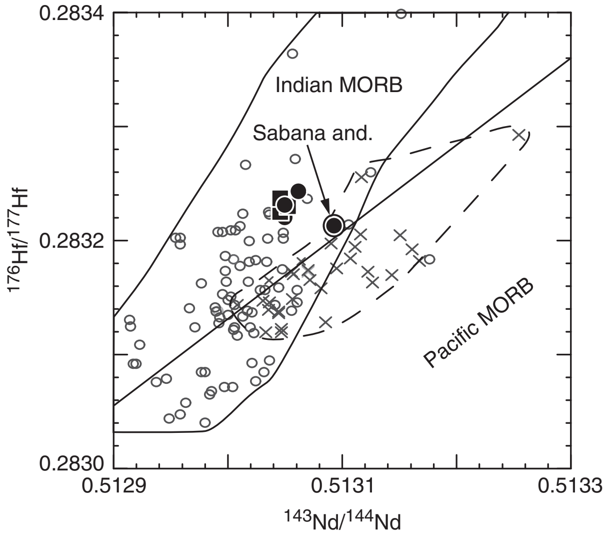

Fig. 12. $^{143}Nd/^{144}Nd$ and $^{176}Hf/^{177}Hf$ variations of MORB from the Indian and Pacific Oceans and the Southeast Indian Ridge, including the Australian–Antarctic Discordance (AAD). In general, Pacific MORB (×) plot below the mantle array regression (continuous straight line; Chauvel & Blichert-Toft, 2001) and define a field (dashed line) that is roughly parallel to it. Indian MORB (○) define a field (continuous line) that cuts obliquely across the mantle array. Symbols for the samples from Saipan and Rota are as in Fig. 6. The measured ratios for the proto-arc (■) and first-arc (●) lavas from Saipan and Rota plot in the Indian MORB field. The Sabana andesite plots in the overlap region between the Indian and Pacific fields, above the mantle array.

Consequently, we use the energy constrained assimilation and fractional crystallization model (EC-AFC) of Bohrson & Spera (2001) to test whether these compositional attributes can be explained by assimilation of young boninitic crust by magmas with normal arc compositions after fore-arc spreading ceased at 45 Ma. The starting composition used in the modeling is a first-arc basaltic andesite from Guam (GUM 80-94). The assimilant is a Site 458 boninite (458 32R-4) from Pearce *et al.* (1999). We compared the model compositions with a Bird Island region rhyolite (SPN02-4). Values for partition coefficients and other parameters used in the modeling are reported in Table 5. The initial temperature for the assimilant was chosen to be 10 degrees below its solidus, which leads to an overall assimilation to crystallization rate ratio (r) of 0·86 and 50% of the original magma mass crystallized when the modeling satisfactorily reproduced the Bird Island rhyolite's trace element pattern. Lower or higher assimilant temperatures caused model trace element patterns that too closely matched either the parental magma or the assimilant. Because of the relatively low overall incompatible trace element abundances after this first stage of modeling, a second stage of 65% Rayleigh fractionation without assimilation was required to approximate the trace element content of the rhyolite (Fig. 14). The high SiO_2 concentrations and the near absence of compatible elements such as V, Ni, Cr, and Cu in these magmas

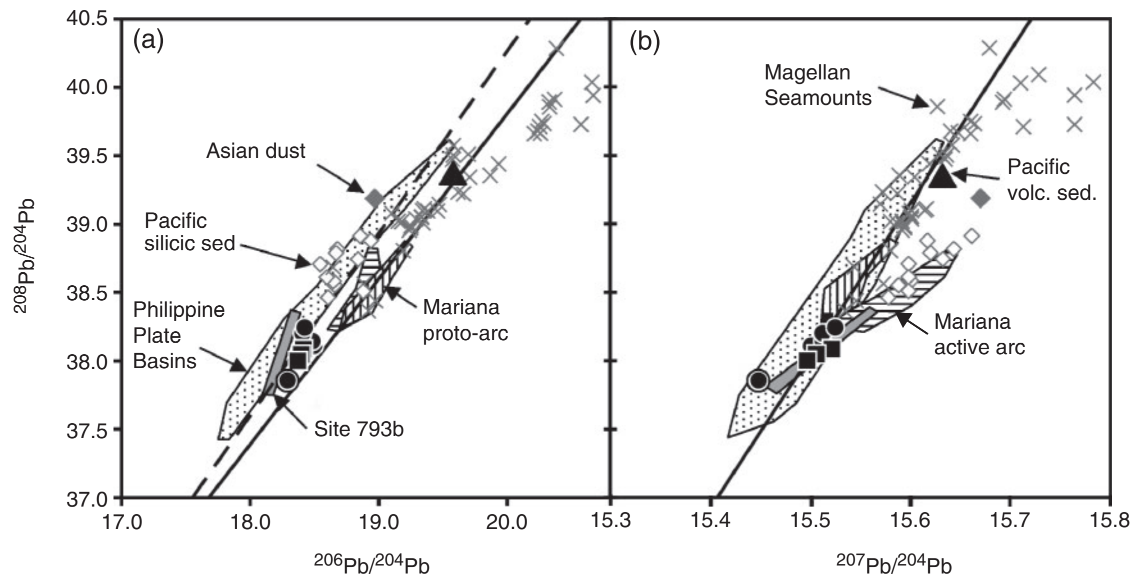

Fig. 13. $^{208}Pb/^{204}Pb$ vs $^{206}Pb/^{204}Pb$ (a) and $^{207}Pb/^{204}Pb$ (b). Most symbols are given in the caption of Fig. 11. Also included are compositions of silicic sediments (◇; Meijer, 1976; Ben Othman *et al.*, 1989), OIB from the Magellan Seamounts (×; Smith *et al.*, 1989; Staudigel *et al.*, 1991), ODP Site 793b (gray shaded area; Taylor *et al.*, 1992), western Pacific volcaniclastic sediment (▲; Pearce *et al.*, 1999) and average late Cenozoic windblown dust from Asia from the western Pacific plate (gray open diamond; Pettke *et al.*, 2000). The continuous diagonal lines represent the Northern Hemisphere Reference Line (NHRL). The dashed line in (a) divides the Pacific and Indian Ocean MORB domains (from Pearce *et al.*, 1999).

Table 4: Representative analyses of adjacent pyroxenes from xenoliths in wt % from Mount Sabana andesite ROT02-8

	Cpx						Opx					
Xenolith no.:	1	1	2	3	5	5	1	1	2	3	5	5
SiO_2	50·72	50·22	51·55	50·88	50·52	50·98	53·93	53·69	53·28	53·74	54·68	54·70
TiO_2	0·38	0·40	0·33	0·33	0·36	0·33	0·15	0·21	0·13	0·17	0·14	0·12
Al_2O_3	3·32	3·66	3·11	2·89	3·19	3·12	2·02	2·03	2·16	2·10	1·29	1·15
Cr_2O_3	0·01	0·00	0·07	0·03	0·03	0·00	0·03	0·03	0·05	0·03	-0·02	0·00
FeO	8·45	9·06	8·12	8·28	8·82	8·33	13·67	14·52	14·07	14·06	13·23	13·25
MnO	0·21	0·19	0·22	0·19	0·22	0·21	0·34	0·37	0·29	0·35	0·37	0·25
MgO	15·80	15·67	16·15	16·06	15·76	16·01	28·31	27·53	27·60	27·97	28·70	28·57
CaO	20·09	19·60	20·26	20·26	19·82	20·05	1·52	1·93	1·55	1·63	1·48	1·49
Na_2O	0·28	0·27	0·22	0·25	0·27	0·27	0·03	0·04	0·02	0·02	0·03	0·02
Total	99·26	99·06	100·04	99·17	98·99	99·29	99·99	100·35	99·17	100·07	99·92	99·55
GPa*	0·36	0·44	0·36	0·24	0·32	0·35						

*Calculated pressure of crystallization (see text).

are consistent with a final stage of pure crystal fractionation. Most model concentrations fall within the range of those shown by the rhyolites. The worst fits are for Nb and Ba, which would have to have been lower and higher respectively in either the intruded magma or the assimilant than in the compositions used in the modeling. The proto-arc rhyolite's Sr–Nd–Hf–Pb composition was also successfully modeled using EC-AFC (Table 5).

The model of rhyolite genesis in the modern Izu–Bonin arc proposed by Tamura & Tatsumi (2002) also has two steps. The first freezes calcalkaline andesites in the crust by devolatilization. The second produces rhyolite by dehydration melting of the resultant amphibole-bearing andesitic plutons. Our first step is similar to theirs, but requires assimilation of boninite crust during fractional crystallization of mantle-derived basalts to elevate LILE abundances over those of REE. In contrast to the Tamura & Tatsumi (2002) model, however, our second step requires crystal fractionation rather than melting. We favor this explanation for the origin of the Sankakuyama Fm. rhyolites, because melting alone would buffer compatible trace elements at measurable values, and would probably occur at pressures that would limit the SiO_2 concentrations in the melt to below the measured values.

Petrogenesis of first-arc lavas

The major element compositions of most first-arc andesites and dacites from Saipan and Rota cannot be generated by crystal fractionation of basalt alone nor by simple mixing between mafic and silicic magma compositions (Fig. 15). Pure crystal fractionation produces trends that are too Fe-enriched during the early stages of differentiation and trends that are too shallow in a plot of FeO*/MgO vs SiO_2 (Fig. 15) once magnetite joins the fractionating assemblage based on MELTS models (e.g. Ghiorso & Sack, 1995; Asimow & Ghiorso, 1998). Mixing mafic and silicic magmas with compositions similar to those of first-arc lavas from Rota and Saipan produces concave-upward trends and, therefore, higher SiO_2 concentrations for a given FeO*/MgO ratio than the observed data. Therefore, the generation of the relatively Fe-enriched compositions of the first-arc andesites and dacites from basaltic parents appears to require crystal fractionation and assimilation of siliceous crust. This hypothesis was tested for major element compositions using MELTS, a first-arc basalt from Guam as the starting composition (NIM80-2), oxygen fugacities buffered at nickel–nickel oxide (NNO), and a low-Si first-arc rhyolite from Guam as the assimilant (GUM02-7). The best fit to the first-arc data was obtained at moderate crustal pressures and water-undersaturated conditions. For example, a model run at 200 MPa, with 2 wt % water in the melt, and an r value of ~0·5 successfully modeled the first-arc compositional variations (Fig. 15). Higher water contents and lower pressures caused precipitation of magnetite at low degrees of fractionation and a more classically calcalkaline trend. The moderate Al_2O_3 concentrations of most first-arc andesites and dacites constrain maximum pressures of fractionation to water-undersaturated conditions at about 300 MPa. The first-arc andesitic samples with the highest Al_2O_3 concentrations (e.g. SPN02-8B with 61·3 wt % SiO_2 and 21·6 wt % Al_2O_3) allow fractionation at higher P and water contents, which both suppress plagioclase fractionation (e.g. Kinzler *et al.*, 2000).

Table 5: Modeling of trace element and isotopic compositions of a proto-arc rhyolite from Saipan

	Bulk *D*		Parent	Assimilant	Model‡	Sample
	EC-AFC	FC	GUM80-94*	458 32R-4†	values	SPN02-4
Rb	0·06	0·12	1·21	6·10	17·60	28·40
K	0·1	0·25	1245	8301	21016	21138
Ba	0·1	0·2	19	20	83	137
Sr	1·1	0·2	139	93	69	72
Pb	0·1	0·3	1·53	0·97	4·96	4·40
Th	0·01	0·02	0·12	0·05	0·46	0·54
U	0·01	0·02	0·10	0·07	0·46	0·48
Nb	0·1	0·3	0·39	0·55	1·87	1·04
La	0·15	0·3	1·38	0·83	4·29	4·85
Nd	0·3	0·3	3·5	1·6	9·0	10·1
Hf	0·1	0·2	0·88	0·66	3·40	3·32
Yb	0·35	0·4	1·48	0·74	3·41	4·10
$^{87}Sr/^{86}Sr°$			0·703554	0·703942	0·703657	0·703520
$^{143}Nd/^{144}Nd°$			0·513023	0·512962	0·513006	0·512986
$^{176}Hf/^{177}Hf°$			0·283202	0·283140	0·283176	0·283213
$^{206}Pb/^{204}Pb$			18·500	18·145	18·376	18·413

*42 Ma basaltic andesite from Guam (Tables 2 and 3).
†48 Ma boninite from DSDP Site 458 (Pearce *et al.*, 1999).
*Using energy constrained assimilation and fractional crystallization (EC-AFC: Bohrson & Spera, 2001) with $r = 0·86$, Mc = 0·5, Cpm = 1450 J/kg K, Cpa = 1400 J/kg K, Hcryst = 390 000 J/kg, Hfus = 350 000 J/kg; followed by 65% fractional crystallization (FC).

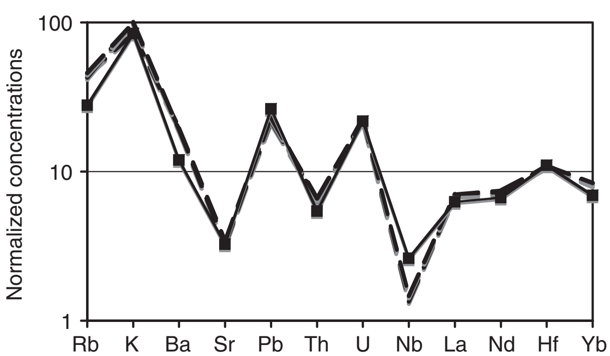

Fig. 14. Primitive mantle-normalized trace element diagram showing model compositions from Table 4 calculated using the energy constrained assimilation and fractional crystallization model (Bohrson & Spera, 2001; Spera & Bohrson, 2001) followed by crystal fractionation (■). A *c.* 42 Ma first-arc tholeiite (GUM 80-94) from Guam is the starting composition and a DSDP Site 458 boninite is the assimilant. The model composition is compared with the compositions of two rhyolites from the Bird Island area of Saipan (nearly overlapping dashed lines).

The trace element and isotopic compositions of the first-arc lavas can be adequately modeled with the EC-AFC model using the trace element pattern of basalt NIM80-2 from Guam as the parent and a first-arc low-Si rhyolite GUM02-7 from Guam as the assimilant, and similar *r* values as for the major element modeling (Table 6, Fig. 16). The initial temperature for the assimilant was chosen to be 60 degrees below its solidus to match the assimilation to crystallization rate ratio ($r = 0·5$) and degree of fractionation ($f = 33\%$) of the major element model when the trace element composition of the first-arc andesites was successfully modeled.

Ratios of highly to moderately incompatible trace elements are high in the websterite-xenolith-bearing samples from the Sabana andesite, despite their significantly less radiogenic Sr and Pb isotopic compositions and more radiogenic Nd compared with the other first-arc andesites. Thus, it appears that the Sabana andesite represents a separate liquid line of descent from the other first-arc lavas. The high MgO concentrations and FeO*/MgO values with respect to SiO_2 concentrations in these lavas are probably due the presence of the websterite xenoliths (e.g. Dungan & Davidson, 2004). However, the steeper REE patterns, lower Ba/La, and higher Sr/Y values for the Sabana andesite compared with other first-arc lavas are unlikely to have resulted from the addition of the pyroxenes making up the websterites. Thus, these features are attributed here to be a primary signature of the parental magmas for these basaltic andesites.

Sources for Sankakuyama Fm. rhyolites

Like other Mariana lavas of all ages, the proto-arc rhyolites from the Sankakuyama Fm. on Saipan lie in the Indian mantle domain on a plot of $^{176}Hf/^{177}Hf$ vs $^{143}Nd/^{144}Nd$ (Fig. 12), indicating that Hf, Nd, and other HFSE and REE were principally derived from the sub-arc mantle of the Philippine Sea plate (see Pearce *et al.*, 1999). Pb isotopic compositions in these lavas, on the other hand, are transitional between the Indian and Pacific domains (Fig. 13). These lavas have high Pb concentrations, indicating that a significant portion of the Pb was derived from the subducting Pacific plate (see also Pearce *et al.*, 1999). Boninitic proto-arc lavas from the Mariana fore-arc have Pb isotope compositions that lie along the Northern Hemisphere Regression Line (NHRL) between the Pacific MORB-like Mount Sabana andesite and those of highly radiogenic Pacific OIB and seafloor volcaniclastic sediments, indicating that fluids from these sources were involved in their genesis (Hickey & Reagan, 1987). The proto-arc rhyolites from Saipan, however, plot with the younger Mariana lavas between a similar less radiogenic end-member and siliceous sediment (Fig. 13), suggesting that these sediments were involved in magma genesis in the region of Saipan during the proto-arc period, as they were at Chichijima (Pearce *et al.*, 1999). The influence of this silicic sediment component clearly expanded towards the transition from proto-arc to first-arc volcanism, when it became the dominant source for radiogenic Pb in the Mariana arc. This expansion probably is related to the

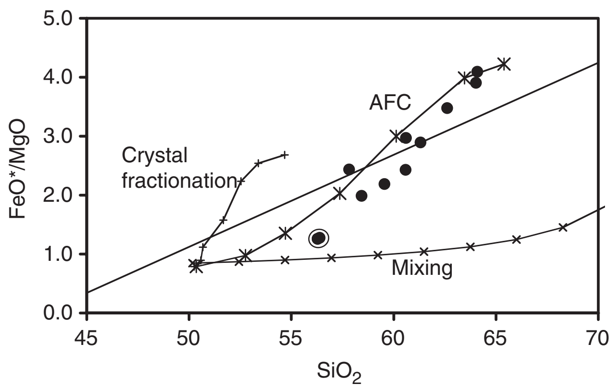

Fig. 15. FeO*/MgO vs SiO_2 illustrating the effects of mixing, crystal fractionation, and assimilation plus fractional crystallization on a first-arc basalt from Guam (NIM 80-2; Hickey-Vargas & Reagan, 1987). ●, first-arc lavas from Saipan and Rota. The Sabana andesite is circled. Division between tholeiite and calc-alkaline series samples after Miyashiro (1974). ×, mixing between the basalt and a proto-arc rhyolite from Saipan in 10% increments; +, crystal fractionation of the basalt using MELTS (Ghiorso & Sack, 1995; run conditions: 200 MPa, NNO, 2 wt % water, model points at 1205, 1165, 1125, 1085, 1045, 1025, and 1005°C). *, AFC fractionation of the basalt with assimilation of first-arc rhyolite GUM 02-7 with 72·8 wt % SiO_2, FeO*/MgO = 2·89, and MgO = 0·96 (run conditions: 200 MPa, NNO, 2 wt % water, model points at 1205, 1145, 1105, 1065, 1025, 985, and 945°C, 5 g of assimilant added at each increment.

Table 6: Modeling of the trace element and isotope compositions of a first-arc andesite from Rota

	Bulk *D* EC-AFC	Parent NIM80-2*	Assimilant GUM02-7†	Model‡ values	Sample ROT02-3b
Rb	0·06	2·44	15·10	17·30	11·60
K	0·1	1494	8024	7497	6307
Ba	0·1	48	99	137	99
Sr	1·1	149	153	138	151
Pb	0·1	0·99	1·91	1·98	2·29
Th	0·01	0·20	0·36	0·53	0·42
U	0·01	0·10	0·23	0·32	0·25
Nb	0·1	0·52	1·37	1·07	0·79
La	0·15	2·42	5·20	4·79	3·99
Nd	0·3	5·3	8·5	8·3	7·0
Hf	0·1	1·16	1·87	2·39	2·28
Yb	0·35	1·62	2·18	2·45	2·61
$^{87}Sr/^{86}Sr^{\circ}$		0·703189	0·703959	0·703284	0·703536
$^{143}Nd/^{144}Nd^{\circ}$		0·512998	0·513006	0·513001	0·513002
$^{176}Hf/^{177}Hf^{\circ}$		0·283200	0·283194	0·283198	0·283209
$^{206}Pb/^{204}Pb$		18·353	18·548	18·442	18·486

*First-arc basalt from Guam (Tables 2 and 3).
†First-arc rhyolite with 72·8 wt % SiO_2 from Guam (Tables 2 and 3).
‡Mc = 0·33, *f* = 0·5 for EC-AFC modeling (see Table 5 for other parameters).

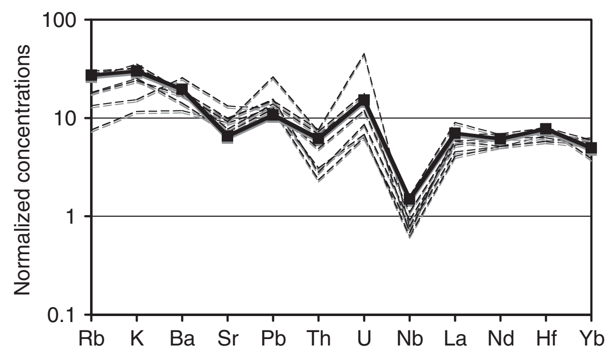

Fig. 16. Primitive mantle-normalized trace element diagram showing model compositions obtained using the energy constrained assimilation and fractional crystallization model (Bohrson & Spera, 2001; Spera & Bohrson, 2001) (■). A first-arc basalt (NIM 80-2) from Guam is the starting composition and first-arc rhyolite GUM 02-7 is the assimilant. The model composition is compared with the compositions of first-arc andesites and dacites from the Hagman Fm. on Saipan and the Ogo volcanics on Rota (dashed lines).

increase in the thickness of windblown sediment from Asia (Pettke *et al.*, 2000).

Boninites and related lavas dominated volcanism in the IBM system from 48 to 44 Ma at DSDP Sites 458 and 459 and on the islands of Chichijima, Palau, and Guam (Meijer *et al.*, 1983; Reagan & Meijer, 1984; Cosca *et al.*, 1998; Mohler, 2003; Reagan *et al.*, 2003). Vigorous mantle upwelling behind the fast sinking Pacific plate was probably the cause for high-degree melting at the low pressures and high water contents (Green, 1973; Falloon & Danyushevsky, 2000; Parman & Grove, 2004) required to produce the extremely depleted boninites at 48–49 Ma (see Stern & Bloomer, 1992). Younger boninites, such as those on Guam, commonly have higher Ca, REE, and HFSE concentrations, suggesting a reduction in the degree of melting with time. As subduction progressed into the late Eocene the drag of the subducting Pacific plate on the overlying mantle might have caused a reversal in the mantle flow beneath the arc to become parallel to the subduction direction (Fig. 17), which would have driven mantle melting to higher pressures (see Stern, 2004). Tholeiitic basalts erupted on Guam at ~42 Ma (Reagan *et al.*, 2003) suggest that pressures of melting were greater and more like those required to produce typical arc basalts 6–8 Myr after subduction initiation at Guam. Ishizuka *et al.* (2006) showed that tholeiitic and calcalkaline basalts and andesites on the Ogasawara Escarpment and Bonin Ridge began erupting as early as 44 Ma, suggesting that a switch to counter-flowing mantle and more typical arc volcanism began to occur there within 4–5 Myr of subduction initiation.

The model above suggests that the change from boninitic to 'normal' arc magma generation processes took place about 3–4 Myr earlier beneath Saipan than beneath Guam. This indicates that rates of arc maturation and changes in mantle flow regimes beneath the nascent IBM system may have varied significantly along the length of the arc. The apparent early initiation of normal subduction-related convection in the mantle wedge (i.e. corner flow) beneath Saipan at 45 Ma may have changed the stress regime of the upper plate and stabilized the crust beneath Saipan, such that it ceased extending and stratified to the point that it could generate rhyolite. This contrasts with Guam, where extensional features such as sheeted dikes and normal faults are associated with boninitic volcanism that continued at least until 44 Ma (e.g. Reagan & Meijer, 1984).

Sources for first-arc lavas

The first-arc lavas from the Mariana fore-arc islands have relatively normal compositions for an island arc setting. They have flat REE patterns, Nb and Ta concentrations that are depleted with respect to LREE, and high concentrations of fluid-mobile elements such as Rb, K, Pb, and U (Fig. 8). The principal source for these lavas was not in the subducted slab, based on the flat REE patterns and the Indian Ocean MORB-like Nd and Hf isotope compositions (Fig. 12). Instead, the less extreme depletion of REE compared with the 48–49 Ma boninites suggests that the primary source for the first-arc parental magmas was relatively enriched Indian Ocean MORB-source mantle. Partial melting to generate the parental magmas of these lavas probably resulted from the addition of a water-rich fluid from the subducting slab. Pb isotope data suggest that this fluid was derived from subducting altered MORB and silicic sediments.

The Sabana andesite from Rota has Nd and Hf isotopic compositions that overlap with Pacific MORB. This andesite also is also considerably more enriched in LREE, more depleted in HFSE, and has ratios between more and less fluid-soluble incompatible elements, suggesting that its parental magma was the product of less fluxing of the source by a water-rich fluid during melting than for other first-arc lavas. The less radiogenic Sr and Pb isotopic compositions of this andesite compared with other first-arc lavas support this contention. One caveat is that the Mount Sabana lava analyzed for its radiogenic isotope composition has a large Ce anomaly and was probably secondarily enriched in most REE (Fig. 8). Its shift in Nd isotopic composition could, therefore, reflect the presence of Nd that was mobilized by weathering. However, there is no obvious source on or near Rota for this radiogenic Nd. We therefore contend that a primary source for incompatible trace elements in these lavas was a melt from subducting Pacific MORB, which reacted with the mantle to generate the parental magma of the Sabana andesites (e.g. Kelemen, 1995). It should be noted that the tight clustering of the proto-arc and other first-arc rocks from the IBM system in the Indian Ocean domain in Fig. 12 indicates that a significant flux of subducted MORB melt to the source of the parental magmas is rare for this arc and that melting of the mantle wedge induced by the fluxing of aqueous fluid driven off the subducting sediment and underlying hydrated mafic to ultramafic oceanic lithosphere is the dominant process for the genesis of IBM magmas.

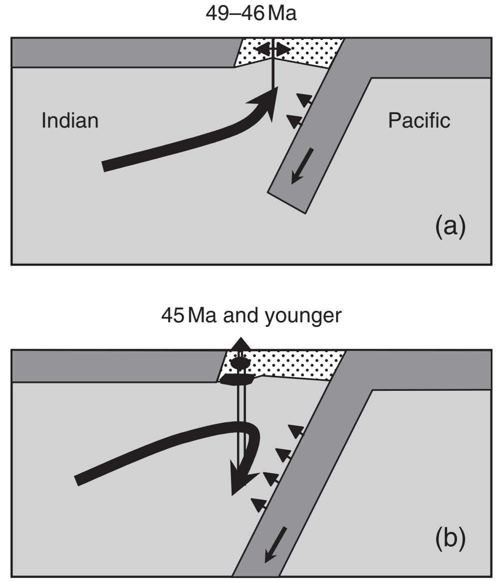

Fig. 17. Schematic illustration of the shift from proto-arc to early-arc volcanism at Saipan. (a) illustrates the upwelling mantle and rift-related boninitic volcanism associated with initial catastrophic sinking of the Pacific plate near the boundary of the Indian and Pacific asthenospheric mantle domains. (b) illustrates the switch to counterflowing asthenospheric mantle, crust stabilization, and normal arc volcanism that occurred at Saipan 3–4 Myr after subduction began, and as much as 7 Myr after subduction began elsewhere in the IBM system.

CONCLUSIONS

A proto-arc rhyolite from the Sankakuyama Fm. on Saipan has an $^{40}Ar/^{39}Ar$ age of 45·1 Ma, indicating that the magmas that form the Sankakuyama Fm. erupted about 3–4 Myr after the boninitic lavas at DSDP Sites 458 and 459 and on the islands of Chichijma and Palau but before the less depleted boninite-series lavas on Guam. Nevertheless, the Saipan rhyolites are geochemically more similar to first-arc lavas erupted at 38 Ma and later on Saipan, Rota, and Guam with their relatively flat REE patterns and large negative Nb and Ta anomalies. Fluids derived from silicic sediments and altered Pacific MORB were both involved in generating the rhyolites and first-arc lavas based on their Pb isotope compositions. REE and HFSE are largely derived from the Philippine plate mantle wedge, based on Hf and Nd isotopic compositions. The Saipan rhyolites were most probably produced by crystal fractionation of tholeiite-series basaltic magmas, similar to those that erupted on Guam at 42 Ma, combined with assimilation of boninitic crust followed by extensive crystal fractionation in the upper crust. This implies that 'normal' arc basalts were involved in magma genesis earlier beneath Saipan than in other portions of the IBM system and only 3–4 Myr after subduction initiation.

The parental magmas of the post-38 Ma lavas in Rota and Saipan were probably generated by partial melting of the sub-Philippine plate mantle wedge in the presence of similar subducted components to those involved in the generation of the proto-arc rhyolites. Differentiation to andesitic and dacitic compositions involved extensive assimilation of predecessor plutons with compositions very much like themselves. The Sabana andesites contrast with the other first-arc lavas in that they have more radiogenic Nd isotopic compositions, which suggest that a melt of subducting Pacific MORB was involved in their genesis. This is the only proto-arc or first-arc lava from the IBM system that clearly has a significant component derived by melting subducted MORB. It also is the youngest of the first-arc lavas studied here, with a disturbed $^{40}Ar/^{39}Ar$ plateau age of 32–33 Ma. We speculate that this time period, which just preceded rifting of the arc to form the Parece Vela Basin, may have been associated with unusually vigorous convection of the mantle wedge and heating of the subducting Pacific plate.

Boninite production during the earliest stages of magmatism has been attributed to fore-arc spreading as hot mantle upwelled into the gap created by the rapidly subducting slab (Stern & Bloomer, 1992; Hall *et al.*, 2003). Significant spreading continued to occur on Guam until about 42 Ma, when arc tholeiites with normal subduction-related trace element characteristics began to erupt. This spreading allowed boninitic magmas to continue to rise to the surface without undergoing significant differentiation. The same transition from boninitic to 'normal' arc magmatism occurred at about 44 Ma in the Bonin Islands region (Ishizuka *et al.*, 2006). In contrast, the island of Saipan shows no evidence of spreading during the Eocene and probably represents crust stabilized by the switch from upwelling to counterflowing mantle. The stabilization of the crust may have allowed differentiation of the parental magmas to silica contents of >77 wt %. By 38 Ma, arc volcanism was occurring throughout the Mariana arc with extensive eruptions of tholeiitic to calc-alkaline basalts, andesites, and dacites on the fore-arc ridge containing the islands of Guam, Saipan, and Rota. This shows that the transition from the fore-arc spreading and mantle upwelling required to generate boninitic parental magmas to counterflowing mantle and limited extension or compression in the arc and fore-arc took between 3 and 7 Myr depending on location.

ACKNOWLEDGEMENTS

Grants OCE0001902, OCE0001824, and OCE0001826 from NSF's MARGINS program funded this work. Discussions between David Peate, Osamu Ishizuka, Robert Stern, Jun-Ichi Kimura, Patricia Fryer, Jennifer Garrison, and the first author helped formulate some of the concepts presented in the manuscript. Adam Kent, Ingrid Ukstins-Peate, and Frank Tepley are thanked for the electron microprobe data. The final paper significantly benefited from the constructive reviews of Julian Pearce, Yoshihiko Tamura, and an anonymous reviewer. Marjorie Wilson's editing considerably improved the paper.

SUPPLEMENTARY DATA

Supplementary data for this paper are available at *Journal of Petrology* online.

REFERENCES

Albarède, F., Télouk, P., Blichert-Toft, J., Boyet, M., Agranier, A. & Nelson, B. (2004). Precise and accurate isotopic measurements using multiple-collector ICPMS. *Geochimica et Cosmochimica Acta* **68**, 2725–2744.

Asimow, P. D. & Ghiorso, M. S. (1998). Algorithmic modifications extending melts to calculate subsolidus phase relations. *American Mineralogist* **83**, 1127–1131.

Ben Othman, D., White, W. M. & Patchett, J. (1989). The geochemistry of marine sediments, island arc magma genesis, and crust–mantle recycling. *Earth and Planetary Science Letters* **94**, 1–21.

Blichert-Toft, J., Chauvel, C. & Albarède, F. (1997). Separation of Hf and Lu for high-precision isotope analysis of rock samples by magnetic sector multiple collector ICP-MS. *Contributions to Mineralogy and Petrology* **127**, 248–260.

Bloomer, S. H. & Hawkins, J. W. (1983). Gabbroic and ultramafic rocks from the Mariana Trench; an island arc ophiolite. In: Hayes, D. E. (ed.) *The Tectonic and Geologic Evolution of Southeast Asian Seas and Islands; Part 2. Geophysical Monograph, American Geophysical Union* **27**, 294–317.

Blundy, J. & Cashman, K. (2001). Ascent-driven crystallization of dacite magmas at Mount St Helens, 1980–1986. *Contributions to Mineralogy and Petrology* **140**, 631–650.

Bohrson, W. A. & Spera, F. J. (2001). Energy-constrained open-system magmatic processes II: Application of energy-constrained assimilation and fractional crystallization (EC-AFC) model to magmatic systems. *Journal of Petrology* **42**, 1019–1041.

Bryant, C. J., Arculus, R. J. & Eggins, S. M. (1999). Laser ablation-inductively coupled plasma-mass spectrometry and tephras; a new approach to understanding arc-magmas genesis. *Geology* **27**, 1119–1122.

Calvert, A. J., Klemperer, S. L., Takahashi, N. & Kerr, B. C. (2005). A 3-D P wave velocity model of the crust and uppermost mantle of the Mariana volcanic arc. *EOS Transactions, American Geophysical Union* **86**, T44A-02.

Carr, M. J., Feigenson, M. D. & Bennett, E. A. (1990). Incompatible element and isotopic evidence for tectonic control of source mixing and melt extraction along the Central American arc. *Contributions to Mineralogy and Petrology* **105**, 369–380.

Chauvel, C. & Blichert-Toft, J. (2001). A hafnium isotope and trace element perspective on melting of the depleted mantle. *Earth and Planetary Science Letters* **170**, 137–151.

Cloud, P. E. J., Schmidt, R. G. & Burke, H. W. (1956). Geology of Saipan. *US Geological Survey, Professional Papers* **221B**, 21–26.

Cosca, M., Arculus, R. J., Pearce, J. A. & Mitchell, J. G. (1998). $^{40}Ar/^{39}Ar$ and K–Ar geochronological age constraints for the inception and early evolution of the Izu–Bonin–Mariana arc system. *Island Arc* **7**, 579–595.

DePaolo, D. J. & Wasserburg, G. J. (1977). The sources of island arcs as indicated by Nd and Sr isotopic studies. *Geophysical Research Letters* **4**, 465–468.

Dobson, P. F. (1986). The petrogenesis of boninite; a field, petrologic, and geochemical study of the volcanic rocks of Chichi-Jima, Bonin Islands, Japan. Ph.D. thesis, Stanford University, 178 pp.

Dungan, M. & Davidson, J. P. (2004). Partial melting at the Earth's surface; implications for assimilation rates and mechanisms in subvolcanic intrusions. *Geology* **32**, 773–776.

Elliott, T., Plank, T., Zindler, A., White, W. & Bourdon, B. (1997). Element transport from slab to volcanic front at the Mariana arc. *Journal of Geophysical Research, B* **102**, 14991–15019.

Falloon, T. J. & Danyushevsky, L. V. (2000). Melting of refractory mantle at 1·5, 2 and 2·5 GPa under anhydrous and H_2O-undersaturated conditions; implications for the petrogenesis of high-Ca boninites and the influence of subduction components on mantle melting. *Journal of Petrology* **41**, 257–283.

Ghiorso, M. S. & Sack, R. O. (1995). Chemical mass transfer in magmatic processes. IV. A revised and internally consistent thermodynamic model for the interpolation and extrapolation of liquid–solid equilibria in magmatic systems at elevated temperatures and pressures. *Contributions to Mineralogy and Petrology* **119**, 197–212.

Gill, J. B. (1981). *Orogenic Andesites and Plate Tectonics*. Berlin: Springer, 390 pp.

Gill, J. B., Hiscott, R. N. & Vidal, P. (1994). Turbidite geochemistry and evolution of the Izu–Bonin arc and continents. *Lithos* **33**, 135–168.

Glazner, A. F. & Ussler, W., III (1989). Crustal extension, crustal density, and the evolution of Cenozoic magmatism in the Basin and Range of the western United States. *Journal of Geophysical Research, B* **94**, 7952–7960.

Graham, D. W., Blichert-Toft, J., Russo, C. J., Rubin, K. H. & Albarède, F. (2006). Cryptic striations in the upper mantle revealed by hafnium isotopes in Southeast Indian Ridge basalts. *Nature* **440**, 199–202.

Green, D. H. (1973). Experimental melting studies on a model upper mantle composition at high pressure under water-saturated and water-undersaturated conditions [Erratum]. *Earth and Planetary Science Letters* **19**, 396.

Hall, C. E., Gurnis, M., Sdrolias, M., Lavier, L. L. & Muller, R. D. (2003). Catastrophic initiation of subduction following forced convergence across fracture zones. *Earth and Planetary Science Letters* **212**, 15–30.

Hanan, B. B. & Schilling, J.-G. (1989). Easter Microplate evolution: Pb isotope evidence. *Journal of Geophysical Research, B, Solid Earth and Planets* **94**, 7432–7448.

Hanan, B. B., Blichert-Toft, J., Pyle, D. & Christie, D. (2004). Contrasting origins of the upper mantle MORB source revealed by Hf and Pb isotopes from the Australian–Antarctic Discordance. *Nature* **432**, 91–94.

Heizler, M. T., Perry, F. V., Crowe, B. M., Peters, L. & Appelt, R. (1999). The age of Lathrop Wells volcanic center: an $^{40}Ar/^{39}Ar$ dating investigation. *Journal of Geophysical Research, B, Solid Earth and Planets* **104**, 767–804.

Hickey-Vargas, R. (1991). Isotope characteristics of submarine lavas from the Philippine Sea; implications for the origin of arc and basin magmas of the Philippine tectonic plate. *Earth and Planetary Science Letters* **107**, 290–304.

Hickey-Vargas, R. (2005). Basalt and tonalite from the Amami Plateau, northern West Philippine Basin: new Early Cretaceous ages and geochemical results, and their petrologic and tectonic implications. *Island Arc* **14**, 653–665.

Hickey-Vargas, R. & Reagan, M. K. (1987). Temporal variation of isotope and rare earth element abundances in volcanic rocks from Guam; implications for the evolution of the Mariana arc. *Contributions to Mineralogy and Petrology* **97**, 497–508.

Hickey-Vargas, R., Abdollahi, M. J., Parada, M. A., Lopez-Escobar, L. & Frey, F. A. (1995). Crustal xenoliths from Calbuco volcano, Andean Southern Volcanic Zone: implications for crustal composition and magma–crust interaction. *Contributions to Mineralogy and Petrology* **119**, 331–344.

Honza, E. & Fujioka, K. (2004). Formation of arcs and backarc basins inferred from the tectonic evolution of Southeast Asia since the Late Cretaceous. *Tectonophysics* **384**, 23–53.

Ishizuka, O., Kimura, J.-I., Li, Y. B., Stern, R. J., Reagan, M. K., Taylor, R. N., Ohara, Y., Bloomer, S. H., Ishii, T., Hargrove, U. S. I. & Haraguchi, S. (2006). Early stages in the evolution of Izu–Bonin arc volcanism: new age, chemical, and isotopic constraints. *Earth and Planetary Science Letters* **250**, 385–401.

Kelemen, P. B. (1995). Genesis of high Mg# andesites and the continental crust. *Contributions to Mineralogy and Petrology* **120**, 1–19.

Kelley, K. A., Plank, T., Ludden, J. N. & Staudigel, H. (2003). Composition of altered oceanic crust at ODP Sites 801 and 1149. *Geochemistry, Geophysics, Geosystems* **4**, paper number 2002GC000435.

Kempton, P. D., Pearce, J. A., Barry, T. L., Fitton, J. G., Langmuir, C. & Christie, D. M. (2002). Sr–Nd–Pb–Hf isotope results from ODP Leg 187: evidence for mantle dynamics of the Australian–Antarctic Discordance and origin of the Indian MORB source. *Geochemistry, Geophysics, Geosystems* **3**, paper number 2002GC000320.

Kinzler, R. J., Donnelly-Nolan, J. M. & Grove, T. L. (2000). Late Holocene hydrous mafic magmatism at the Paint Pot Crater and Callahan Flows, Medicine Lake Volcano, N. California and the influence of H_2O in the generation of silicic magmas. *Contributions to Mineralogy and Petrology* **138**, 1–16.

Kitamura, K., Ishikawa, M. & Arima, M. (2003). Petrological model of the northern Izu–Bonin–Mariana arc crust: constraints from high-pressure measurements of elastic wave velocities of the Tanzawa plutonic rocks, central Japan. *Tectonophysics* **371**, 213–221.

Kodaira, S., Sato, T., Takahashi, N., Miura, S., Tamura, Y., Tatsumi, Y. & Kaneda, Y. (2007). New seismological constraints on growth of continental crust in the Izu–Bonin intra-oceanic arc. *Geology* **35**, 1031–1034.

Kohut, E. J., Stern, R. J., Kent, A. J. R., Nielsen, R. L., Bloomer, S. H. & Matthew, L. (2006). Evidence for adiabatic decompression melting in the southern Mariana arc from high-Mg lavas and melt inclusions. *Contributions to Mineralogy and Petrology* **152**, 201–221.

Kuiper, Y. D. (2002). The interpretation of inverse isochron diagrams in $^{40}Ar/^{39}Ar$ geochronology. *Earth and Planetary Science Letters* **203**, 499–506.

Meijer, A. (1976). Pb and Sr isotopic data bearing on the origin of volcanic rocks from the Mariana Island-Arc system. *Geological Society of America Bulletin* **87**, 1358–1369.

Meijer, A. (1983). The origin of low-K rhyolites from the Mariana frontal arc. *Contributions to Mineralogy and Petrology* **83**, 45–51.

Meijer, A., Reagan, M., Ellis, H., Shafiqullah, M., Sutter, J., Damon, P. & Kling, S. (1983). Chronology of volcanic events in the eastern Philippine Sea. In: Hayes, D. E. (ed.) *The Tectonic and Geologic*

Evolution of Southeast Asian Seas and Islands; Part 2. Geophysical Monograph, American Geophysical Union **27**, 349–359.

Miyashiro, A. (1974). Volcanic rock series in island arcs and active continental margins. *American Journal of Science* **274**, 321–355.

Mohler, D. A. (2003). *Geochronology, Petrology, and Geochemistry of Volcanic Rocks on Guam*. Iowa City: Department of Geoscience, University of Iowa, 68 pp.

Nimis, P. (1999). Clinopyroxene geobarometry of magmatic rocks part 2: Structural geobarometers for basic to acid, tholeiitic and mildly alkaline magmatic systems. *Contributions to Mineralogy and Petrology* **135**, 62–74.

Nimis, P. & Ulmer, P. (1998). Clinopyroxene geobarometry of magmatic rocks part 1: An expanded structural geobarometer for anhydrous and hydrous, basic and ultrabasic systems. *Contributions to Mineralogy and Petrology* **133**, 122–135.

Parman, S. W. & Grove, T. L. (2004). Harzburgite melting with and without H_2O; experimental data and predictive modeling. *Journal of Geophysical Research (B)* **109**, paper number 2003JB002566.

Patino, L. C., Velbel, M. A., Price, J. R. & Wade, J. A. (2003). Trace element mobility during spheroidal weathering of basalts and andesites in Hawaii and Guatemala. *Chemical Geology* **202**, 343–364.

Pearce, J. A., Thirlwall, M. F., Ingram, G., Murton, B. J., Arculus, R. J. & van der Laan, S. R. (1992). Isotopic evidence for the origin of boninites and related rocks drilled in the Izu-Bonin (Ogasawara) fore-arc, Leg 125. In: Fryer, P., Pearce, J. A., Stokking, L. B., *et al.* (eds) *Proceedings of the Ocean Drilling Program, Scientific Results, 125.* College Station, TX: Ocean Drilling Program, pp. 237–261.

Pearce, J. A., Kempton, P. D., Nowell, G. M. & Noble, S. R. (1999). Hf–Nd element and isotope perspective on the nature and provenance of mantle and subduction components in western Pacific arc–basin systems. *Journal of Petrology* **40**, 1579–1611.

Pettke, T., Halliday, A. N., Hall, C. M. & Rea, D. K. (2000). Dust production and deposition in Asia and the North Pacific Ocean over the past 12 Myr. *Earth and Planetary Science Letters* **178**, 397–413.

Plank, T. & Ludden, J. N. (1992). Geochemistry of sediments in the Argo Abyssal Plain at Site 765; a continental margin reference section for sediment recycling in subduction zones. In: Gradstein, F. M. & Ludden, J. N. (eds) *Proceedings of the Ocean Drilling Program, Scientific Results, 123.* College Station, TX: Ocean Drilling Program, pp. 167–189.

Reagan, M. K. & Gill, J. B. (1989). Coexisting calcalkaline and high-niobium basalts from Turrialba volcano, Costa Rica; implications for residual titanates in arc magma sources. *Journal of Geophysical Research, B* **94**, 4619–4633.

Reagan, M. K. & Meijer, A. (1984). Geology and geochemistry of early arc-volcanic rocks from Guam. *Geological Society of America Bulletin* **95**, 701–713.

Reagan, M., Mohler, D., Hanan, B., Hickey-Vargas, R. & Blichert-Toft, J. (2003). Sources and melting processes for the proto-Mariana arc. *Geophysical Research Abstracts* **5**, 14493.

Schilling, J.-G., Hanan, B. B., McCully, B., Kingsley, R. H. & Fontignie, D. (1994). Influence of the Sierra Leone mantle plume on the Equatorial Mid-Atlantic Ridge: a Nd–Sr–Pb isotopic study. *Journal of Geophysical Research, B* **99**, 12005–12028.

Shukuno, H., Tamura, Y., Tani, K., Chang, Q., Suzuki, T. & Fiske, R. S. (2006). Origin of silicic magmas and the compositional gap at Sumisu submarine caldera, Izu–Bonin arc, Japan. *Journal of Volcanology and Geothermal Research* **156**, 187–216.

Smith, W. H. F., Staudigel, H., Watts, A. B. & Pringle, M. S. (1989). The Magellan Seamounts: Early Cretaceous record of the South Pacific isotopic and thermal anomaly. *Journal of Geophysical Research, B* **94**, 10501–10523.

Spera, F. J. & Bohrson, W. A. (2001). Energy-constrained open-system magmatic processes I: general model and energy-constrained assimilation and fractional crystallization (EC-AFC) formulation. *Journal of Petrology* **42**, 999–1018.

Staudigel, H., Park, K.-H., Pringle, M. S., Rubenstone, J. L., Smith, W. H. F. & Zindler, A. (1991). The longevity of the South Pacific isotopic and thermal anomaly. *Earth and Planetary Science Letters* **102**, 24–44.

Stern, R. J. (2004). Subduction initiation; spontaneous and induced. *Earth and Planetary Science Letters* **226**, 275–292.

Stern, R. J. & Bloomer, S. H. (1992). Subduction zone infancy; examples from the Eocene Izu–Bonin–Mariana and Jurassic California arcs. *Geological Society of America Bulletin* **104**, 1621–1636.

Stern, R. J., Fouch, M. J. & Klemperer, S. L. (2003). An overview of the Izu–Bonin–Mariana Subduction Factory. In: Eiler, J. (ed.) *Inside the Subduction Factory. Geophysical Monograph, American Geophysical Union* **138**, 175–222.

Straub, S. M. (2003). The evolution of the Izu Bonin–Mariana volcanic arcs (NW Pacific) in terms of major element chemistry. *Geochemistry, Geophysics, Geosystem* **4**, paper number 2002GC000357.

Sun, S. S. & McDonough, W. F. (1989). Chemical and isotopic systematics of oceanic basalts: implications for mantle composition and processes. In: Saunders, A. D. & Norry, M. J. (eds) *Magmatism in the Ocean Basins. Geological Society, London, Special Publications* **42**, 315–345.

Suyehiro, K., Takahashi, N. & Ariie, Y. (1996). Continental crust, crustal underplating, and low-Q upper mantle beneath an oceanic island arc. *Science* **272**, 390–392.

Takahashi, N., Suyehiro, K. & Shinohara, M. (1998). Implications from the seismic crustal structure of the northern Izu–Bonin arc. *Island Arc* **7**, 383–394.

Takahashi, N., Kodaira, S., Klemperer, S. L., Tatsumi, Y., Kaneda, Y. & Suyehiro, K. (2007). Crustal structure and evolution of the Mariana intra-oceanic island arc. *Geology* **35**, 203–206.

Tamura, Y. & Tatsumi, Y. (2002). Remelting of an andesitic crust as a possible origin for rhyolitic magma in oceanic arcs: an example from the Izu–Bonin Arc. *Journal of Petrology* **43**, 1029–1047.

Tayama, R. (1938). Geomorphology, geology, and coral reefs of Saipan Island. *Tropical Industries Institution Bulletin* **1**, 1–62.

Taylor, R. N., Lapierre, H., Vidal, P., Nesbitt, R. W. & Croudace, I. W. (1992). Igneous geochemistry and petrogenesis of the Izu-Bonin Forearc Basin. In: Taylor, B., Fujioka, K. *et al.* (eds) *Proceedings of the Ocean Drilling Program, Scientific Results* **126**, 405–430.

Taylor, R. N., Nesbitt, R. W., Vidal, P., Harmon, R. S., Auvray, B. & Croudace, I. W. (1994). Mineralogy, chemistry, and genesis of the boninite series volcanics, Chichijima, Bonin Islands, Japan. *Journal of Petrology* **35**, 577–617.

Todt, W., Cliff, R. A., Hanser, A. & Hofmann, A. W. (1996). Evaluation of a ^{202}Pb–^{205}Pb double spike for high precision lead isotope analysis. In: Hart, S. R. & Basu, A. (eds) *Earth Processes: Reading the Isotope Code. Geophysical Monograph, American Geophysical Union* **95**, 429–437.

Tracey, J. I., Schlanger, S. O., Stark, J. T., Doan, D. B. & May, H. G. (1964). *General Geology of Guam. US Geological Survey, Professional Papers* **403A**, 104 pp.

Umino, S. (1985). Volcanic geology of Chichijima, the Bonin Islands (Ogasawara Islands). *Journal of the Geological Society of Japan* **91**, 505–523.

White, W. M., Albarède, F. & Télouk, P. (2000). High-precision analysis of Pb isotope ratios by multicollector ICP-MS. *Chemical Geology* **167**, 257–270.

Woodhead, J. D., Hergt, J. M., Davidson, J. P. & Eggins, S. M. (2001). Hafnium isotope evidence for 'conservative' element mobility during subduction zone processes. *Earth and Planetary Science Letters* **192**, 331–346.

York, D. (1969). Least squares fitting of a straight line with correlated errors. *Earth and Planetary Science Letters* **5**, 320–324.